

A large radio nebula around P Cygni

C. J. Skinner,^{1,2,3*} R. H. Becker,^{2,4} R. L. White,¹ K. M. Exter,⁵ M. J. Barlow^{6,†}
and R. J. Davis⁷

¹*Space Telescope Science Institute, 3700 San Martin Drive, Baltimore, MD 21218, USA*

²*Institute of Geophysics & Planetary Physics, L-413, Lawrence Livermore National Laboratory, PO Box 808, Livermore, CA 94551-9900, USA*

³*Laboratory for Experimental Astrophysics, Lawrence Livermore National Laboratory, PO Box 808, Livermore, CA 94551-9900, USA*

⁴*Department of Physics, University of California, Davis, CA 95616, USA*

⁵*Department of Physics & Astronomy, University of St Andrews, North Haugh, St Andrews, Fife KY16 9SS*

⁶*Department of Physics & Astronomy, University College London, Gower Street, London WC1E 6BT*

⁷*Nuffield Radio Astronomy Laboratories, Jodrell Bank, Macclesfield, Cheshire SK5 9DL*

Accepted 1997 December 12. Received 1997 November 3; in original form 1996 November 15

ABSTRACT

We present a large set of radio observations of the luminous blue variable P Cygni. These include two 6-cm images obtained with MERLIN which spatially resolve the 6-cm photosphere, monitoring observations obtained at Jodrell Bank every few days over a period of two months, and VLA observations obtained every month for seven years. This combination of data shows that the circumstellar environment of P Cyg is highly inhomogeneous, that there is a radio nebula extending to almost an arcminute from the star at 2 and 6 cm, and that the radio emission is variable on a time-scale no longer than one month, and probably as short as a few days. This short-time-scale variability is difficult to explain. We present a model for the radio emission with which we demonstrate that the star has probably been losing mass at a significant rate for at least a few thousand years, and that it has undergone at least two major outbursts of increased mass loss during the past two millenia.

Key words: circumstellar matter – stars: individual: P Cyg – stars: mass-loss – stars: variables: other – radio continuum: stars.

1 INTRODUCTION

P Cygni is a hot star ($T_{\text{eff}} \sim 20\,000$ K; Barlow & Cohen 1977) with many unusual properties. Its mass and evolutionary status are not certain (e.g. Pauldrach & Puls 1990; El Eid & Hartmann 1993), but it is believed to be a member of the IC 4996 open cluster (Lamers, de Groot & Cassatella 1983). At a presumed distance of 1.8 kpc (based on its presumed IC 4996 membership) it has an absolute visual magnitude of -8.3 and a luminosity of more than $7 \times 10^5 L_{\odot}$. With such prodigious vital statistics, P Cyg is probably a member of the small group of extremely massive hypergiants known as luminous blue variables (LBVs; Conti 1984; Humphreys 1989). LBVs have heavily N-enriched circumstellar envelopes, formed by mass loss in stellar winds, indicative that the stellar atmospheres have been chemically altered by CNO-cycle processing (e.g. Davidson et al. 1986; Nota et al. 1992; Clampin et al. 1993).

LBVs are violently unstable stars, prone to episodes of very heavy mass loss. The prototype η Carinae had a formidable outburst around AD 1843, becoming the second brightest star in the sky, and forming a spectacular optical nebula known as the Homunculus.

η Car is still losing mass at a rate of the order of $10^{-3} M_{\odot} \text{ yr}^{-1}$ (Davidson et al. 1986). Other LBVs have also generated impressive optical nebulae, although their optical photometric histories are less well known. P Cyg, like η Car, is known to have undergone major outbursts in recorded history. It was more or less unknown until it underwent an outburst in AD 1600 during which it became a third-magnitude star, and it experienced a second brightening in AD 1655 (de Groot 1969). Since 1700 it has been observed many times, and appears to have been slowly brightening at visible wavelengths (Lamers & de Groot 1992).

Unlike all of the known LBVs, P Cyg did not until recently appear to possess any optical nebula. However, Leitherer & Zickgraf (1987) found some evidence for extension in H α and [N II] emission lines out to about 7 arcsec from the star, which they attributed to matter ejected in dense shells. Johnson et al. (1992) observed a variety of nebular emission lines in long-slit spectra at a position offset 9 arcsec from the star. These revealed an electron density 20 times larger than predicted by expansion of the present-day wind, and very heavy N enrichment of the wind, in keeping with the properties of known LBVs. They also discovered anomalously strong [Ni II] emission. Finally, Barlow et al. (1994) obtained coronagraphic images of P Cyg in the [N II] $\lambda 6584$ line, which revealed a bright emission nebula with a radius of ~ 11 arcsec, and

*Deceased 1997 October 21.

†Author for offprint requests.

fainter outer arcs of emission with radii of 30 and 45 arcsec. The Barlow et al. long-slit spectra hint at the presence of structure closer to the star, with a radius of ~ 6 arcsec (too close to the star to be seen in the coronagraph images), which may be attributable to the 17th-century outbursts. With the discovery of its large optical nebula, P Cyg now resembles much more closely the other LBVs, increasing the likelihood that it too is an LBV.

The wind of P Cyg exhibits a complex ensemble of properties at optical and UV wavelengths. Velocities ranging from 400 km s^{-1} (Underhill 1979) to only 100 km s^{-1} (Barlow et al. 1994) have been observed in the wind. The latter authors proposed that the lower velocity, which is seen in a number of low-excitation lines, corresponds to dense blobs ejected during an outburst. These blobs are impacted by the wind flowing at a terminal velocity a little faster than 200 km s^{-1} (Lamers, Korevaar & Cassatella 1985; Barlow et al. 1994), generating a bow shock and the apparently high electron densities and temperatures. Lamers et al. (1985) observed time-variable iron absorption lines in *IUE* spectra of P Cyg, which seemed to indicate the ejection of dense shells with a recurrence time of order a year.

The mass-loss rate for P Cyg can be estimated by various techniques. Infrared photometry (e.g. Barlow & Cohen 1977), optical spectra (e.g. Klein & Castor 1978), UV spectra (Lamers et al. 1985) and radio photometry (e.g. Abbott, Bieging & Churchwell 1981) can all be used to determine a mass-loss rate for this star. The techniques all yield values of order $1\text{--}3 \times 10^{-5} M_{\odot} \text{ yr}^{-1}$, which is large for an early B supergiant but quite low for an LBV.

P Cyg was one of the first radio stars to be detected (Wendker, Baars & Altenhoff 1973). A variety of observations soon suggested that it was a variable radio source (Abbott et al. 1981). van den Oord et al. (1985) presented a five-year series of observations at a wavelength of 6 cm, showing that P Cyg varies from as little as 1.6 mJy to almost 11 mJy. The time-scale for the variations appeared to be no more than a few months. With a terminal velocity of only 206 km s^{-1} (Lamers et al. 1985), the time-scale for a change in mass-loss rate to permeate the region responsible for the 6-cm flux is several years, so that changes in mass-loss rate cannot be responsible for the variable flux. Instead, van den Oord et al. proposed that the radio emission was modulated by the dense shells postulated by Lamers et al. (1985): changes in optical depth in the wind caused by ejection of these dense shells would lead to a variable ionization fraction and hence electron density. However, new work presented by Skinner et al. (1997b) has cast significant doubt on this mechanism.

The physical size of the P Cyg radio source is uncertain. Abbott et al. (1980) presented data which appeared to indicate extension at 6 cm, although they did not really believe it. With much longer baselines, Abbott et al. (1981) detected much less flux. This ought to have raised the possibility that P Cyg is significantly extended at radio wavelengths, since very long baselines are insensitive to very extended structure. None the less, researchers continue to assume that P Cyg is basically a point source, driven by the expectations of a simple ionized stellar wind model (Wright & Barlow 1975; Panagia & Felli 1975). Repeated detection of very extended emission around P Cyg (Wendker 1982; Baars & Wendker 1987) did not dent the pre-conceived notion that P Cyg must be a point source. The multifrequency observations by Baars & Wendker (1987) clearly reveal that the P Cyg radio source comprises both a compact core and a more extended arc or halo, of order an arcminute in size, which appears to be thermal in origin. As long ago as 1982, White & Becker showed that even the compact core is resolved by the VLA in its highest spatial resolution ‘A’ configuration. Given such a

structure, it is clear that observations by radio interferometers with different baselines may obtain different fluxes for P Cyg, and so the discussion of source variability by van den Oord et al. (1985) must be treated with some caution.

To understand better the radio structure and possible variability of P Cyg, we have made a large number of radio observations. These include monitoring the radio flux at two wavelengths on a monthly basis for a period of seven years, monitoring at only one wavelength on an almost daily basis for a period of two months, and making very high signal-to-noise ratio (S/N) and very high spatial resolution radio images.

2 DAILY MONITORING AT 6 CM

Radio observations of P Cyg in the past have typically been separated by many months. To constrain better our understanding of the time-scale for variability, we observed the star frequently over a period of roughly 70 d at a wavelength of 6 cm (5.0-GHz frequency), using the Broad Band Interferometer (BBI) at Jodrell Bank. The BBI comprises the Lovell (76m) and Mk II ($38 \times 26 \text{ m}^2$) telescopes with a baseline of 424 m, and is described in detail by Padin, Davis & Lazenby (1987). The system temperature for the receivers was about 35 K. The spatial resolution, determined by the baseline, is about 30 arcsec. The observations were made in the period 1990 December to 1991 February. The VLA calibrator 2005+403 was used as a phase and amplitude calibrator, with its flux density set to 2.770 Jy (an average of three MERLIN results). The primary calibrator was 3C 286. Typically integrations on P Cyg lasted about an hour, and the calibrator was observed immediately before and after, so that any possible changes in gain or phase behaviour could be determined.

Before presenting the results, it is important to discuss the uncertainties in the data, so that a quantitative estimate of the significance of any apparent variability can be assessed. A significant source of amplitude instability for the BBI is tracking errors by the Lovell telescope. To avoid this, telescope pointing is monitored, and data acquired when the pointing error was greater than a fraction of the Lovell beamwidth is rejected. The amplitude stability of the BBI for 1-h integrations is determined to be about 3 per cent. Short-term phase instability is dominated by the atmosphere. Longer term phase drifts are removed by phase calibration, and residual phase errors are found to be generally less than 5° . Finally, thermal noise is estimated to contribute an uncertainty of about 0.4 mJy to all the measurements.

The resulting 6-cm light curve for P Cyg is presented as Fig. 1. Every datum has been individually checked for reliability. A few observations that have slightly larger uncertainties are discussed here.

In the observations on JD 244 8275.0 and 244 8276.1, sinusoidal structure was evident in the phase and amplitude of P Cyg, as though another source were present in the beam about 10 arcmin from P Cyg. However, because of the sinusoidal pattern, the effects seem to have been self-cancelling, and so we believe these data to have uncertainties only marginally greater than that estimated above for the majority of the observations.

On JD 244 8303.8 and 244 8305.8 the system sensitivities appeared suddenly to change during the P Cyg integrations. Careful re-analysis of these observations suggests that there is an additional few per cent uncertainty on the resulting fluxes.

If we disregard the extreme datum of JD 244 8296.2, the mean flux obtained with the BBI was 7.07 ± 0.45 mJy, consistent with the mean flux of 6.7 mJy obtained by van den Oord et al. (1985). The

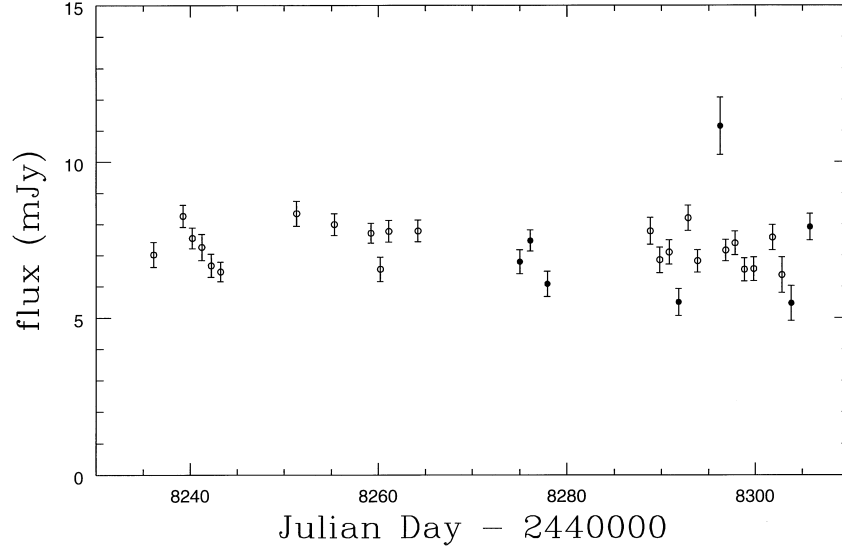


Figure 1. Jodrell Bank BBI 6-cm observations of P Cyg.

standard deviation of these data is 0.64 mJy, suggesting that the source is varying typically by ± 9 per cent about the mean, while careful tests of the amplitude stability of the BBI indicate that, as mentioned earlier, it should impart only a ± 3 per cent uncertainty. At least one datum (JD 244 8296.2) indicates that variations as large as 60 per cent may occasionally occur on a time-scale as short as a day. The trough-to-peak difference is 5.69 mJy if we include the highest point, or 2.88 mJy if we do not, so that we see variations as large as ± 20 per cent quite frequently. The largest variation is the JD 244 8296.2 datum, where over the course of about 4 days the observed flux rose by about 50 per cent and then fell again. The available calibration data, and observations of other sources close in time to this, do not suggest any instrumental or environmental cause, and so it appears that this is a real variation by the source.

We must consider that either the apparent variability we see here is due to calibration uncertainties, or the star really displays significant radio variability on a remarkably short time-scale. To test this, we used a statistical test designed to determine the probability of two different variances arising from the same population, namely the F-test (e.g. Goodman 1957; Bevington & Robinson 1992). Using the two variances found here (3 per cent for the BBI amplitude stability and 9 per cent for the P Cyg observations), the F-test indicates that the probability of these two variances both arising in the same population is less than 1 per cent. This means that it is almost certain that the two variances arose in different ways, one owing to noise, and the other owing to source variability. Finally, for random observations of a given source, half of the observations are expected to fall in the range $\mu \pm \epsilon$, where μ is the mean result and ϵ the probable error (e.g. Bevington & Robinson 1992). We find that, for our BBI observations of P Cyg, less than 30 per cent of the results fall within the probable error on the mean. Thus every means of analysis of these data indicates that P Cyg varies typically by up to 20 per cent on a time-scale of a few days. Such behaviour would not at first glance appear to be consistent with the model of van den Oord et al. (1985). This will be discussed later.

3 HIGH SPATIAL RESOLUTION 6-CM IMAGES

We used MERLIN (the Multi-Element Radio-Linked Interferometer

Network) to obtain high spatial resolution images of P Cyg at a wavelength of 6 cm (a frequency of 5.0 GHz). These data have been described in more detail by Skinner et al. (1997b), and so are only summarized here. Observations were made on 1992 June 24 and August 04. In each case the beamsize was $48 \times 51 \text{ mas}^2$. Because the shortest MERLIN baseline is 11 km, components of the source significantly more extended than about 0.1 arcsec will not be detected.

The two images are presented in Figs 2 and 3. It is clear that dramatic changes have occurred on a time-scale of 40 d. To see whether the fluxes, as well as the overall structure, have changed, further images were made with the beam tapered to a 0.3-arcsec circle. The resulting images were found to be reasonably well fitted by an elliptical $0.3 \times 0.4 \text{ arcsec}^2$ Gaussian, and resulting fluxes are listed in Table 1. Evidently the flux has changed by more than 1 mJy (or 25 per cent). This is comparable with the variability seen in our BBI observations.

The characteristic diameter of the radio photosphere for P Cyg at 6 cm is predicted to be about 0.10 arcsec by equation (11) of Wright & Barlow (1975), which is about two-thirds of the size of the region delineated by the MERLIN images. The 6-cm emission appears to arise in a chaotic region with a typical size of a little less than 0.2 arcsec. This corresponds, at a distance of 1.8 kpc, to a radius of roughly $500 R_*$, where R_* , the stellar photospheric radius, is estimated to be $76 R_\odot$ (Lamers et al. 1983).

4 LONG-TERM 2- AND 6-CM MONITORING

We have used the NRAO Very Large Array (VLA) to observe P Cyg at roughly monthly intervals at wavelengths of 2 cm (a frequency of 14.965 GHz) and 6 cm (4.8851-GHz frequency), from 1986 September to 1993 January. The VLA is operated in four array configurations, denoted A, B, C and D. In changing to successively more compact array configurations from A to D, the antennas are moved steadily closer together, so that as the array cycles from A through to D progressively shorter baselines are sampled. The array spends 4 months in each configuration, thus the cycle time is 16 months. Our monitoring spans approximately 5 cycles, so we have an excellent opportunity to investigate the effect of baseline changes on the observed flux of P Cyg. If the star is, as generally claimed, a radio point source, then changing array configurations

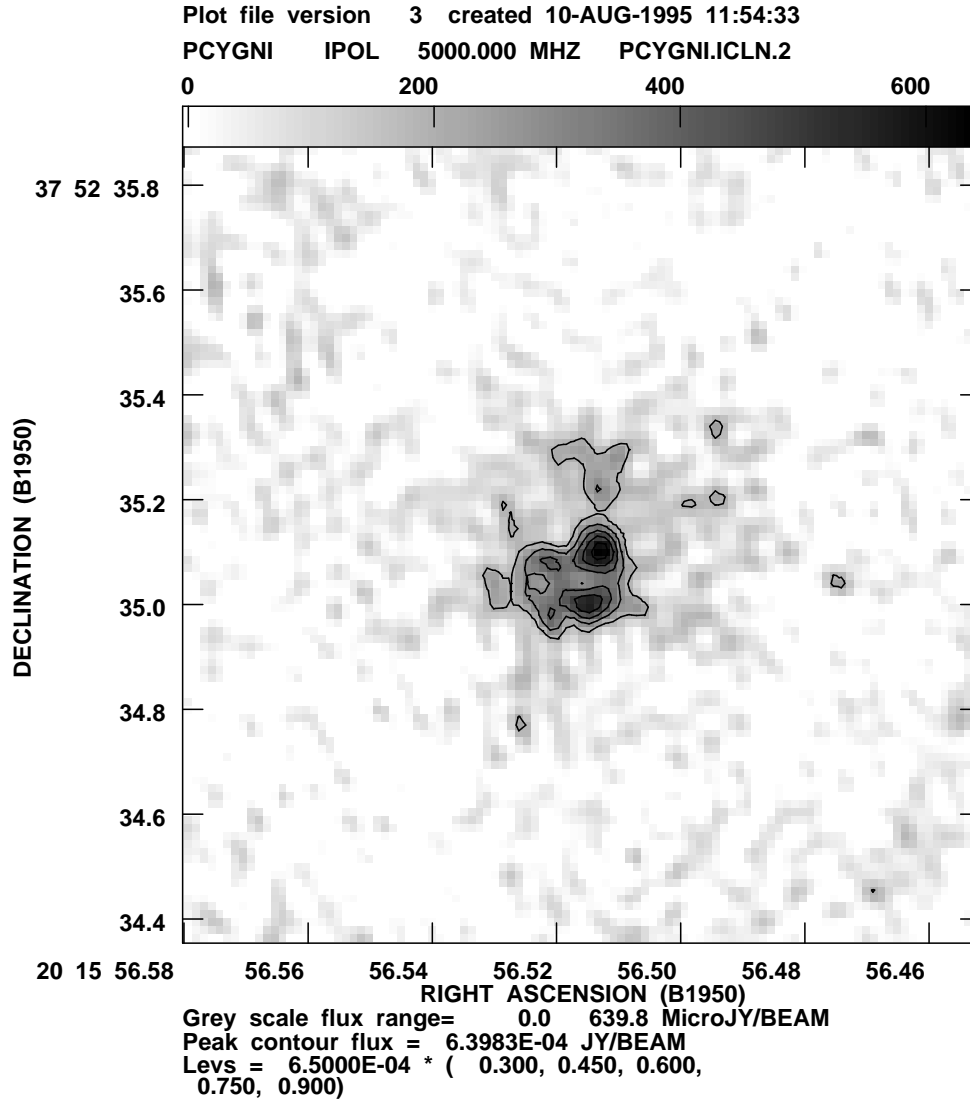


Figure 2. 6-cm MERLIN image of P Cyg from 1992 June 24. The synthesized beam is an ellipse of FWHM size $48 \times 51 \text{ mas}^2$.

should make no difference to the flux. For a given minimum baseline, there is a corresponding maximum size structure that can be detected with an interferometer: any structure larger than this will be ‘lost’ in resulting images. In Table 2 we summarize the half-power beamwidths θ_b (which may be used as an indication of the spatial resolution achievable) and corresponding largest detectable structures θ_{max} for the VLA’s four configurations.

On each date one observation was made at each wavelength of a VLA primary calibrator (usually 3C 48), and a number of observations of the secondary calibrator 2005+403. For each observation, we have used the standard reduction tasks in the NRAO AIPS package to calibrate the uv data, transform them to a map and clean it. Fluxes were then determined by fitting a Gaussian to the radio source and integrating the flux under the Gaussian. The results are displayed in Fig. 4.

A number of points are immediately clear from Fig. 4. Foremost, the fluxes measured at different times are very different, in accord with our observations presented earlier. Secondly, most of the smallest fluxes were recorded with the array in A configuration, while most of the largest were recorded in D configuration. This effect is particularly prominent in the 6-cm observations. By

implication, the radio source must be quite extended. Following the example of White & Becker (1982), to check for source extension we looked at the visibility curves for each observation. The visibility curves for A and D array configurations, obtained by averaging the entire seven years’ observations for each array configuration, are presented in Fig. 5, and it can be seen that not only is the radio source heavily resolved in A configuration, as described by White & Becker, but also it is quite clearly resolved in D configuration. Since the half-power beamwidth in D configuration is 14 arcsec, the implication is that the radio source must be very large. Such an effect should have been easily seen in the data of the many previous observers of P Cyg, provided that the S/N was reasonable. A third point evident from Fig. 4 is that for a fixed array configuration there appears to be significant variability, so that the reports of variability by previous workers are not (necessarily) invalidated by the source extension. Finally, we have plotted the BBI monitoring observations in Fig. 4, and it seems that the BBI fluxes and those seen very soon after by the VLA in C configuration are in good agreement.

We wish to achieve two goals using our seven years of observations from the VLA. First, we wish to determine the level of any real

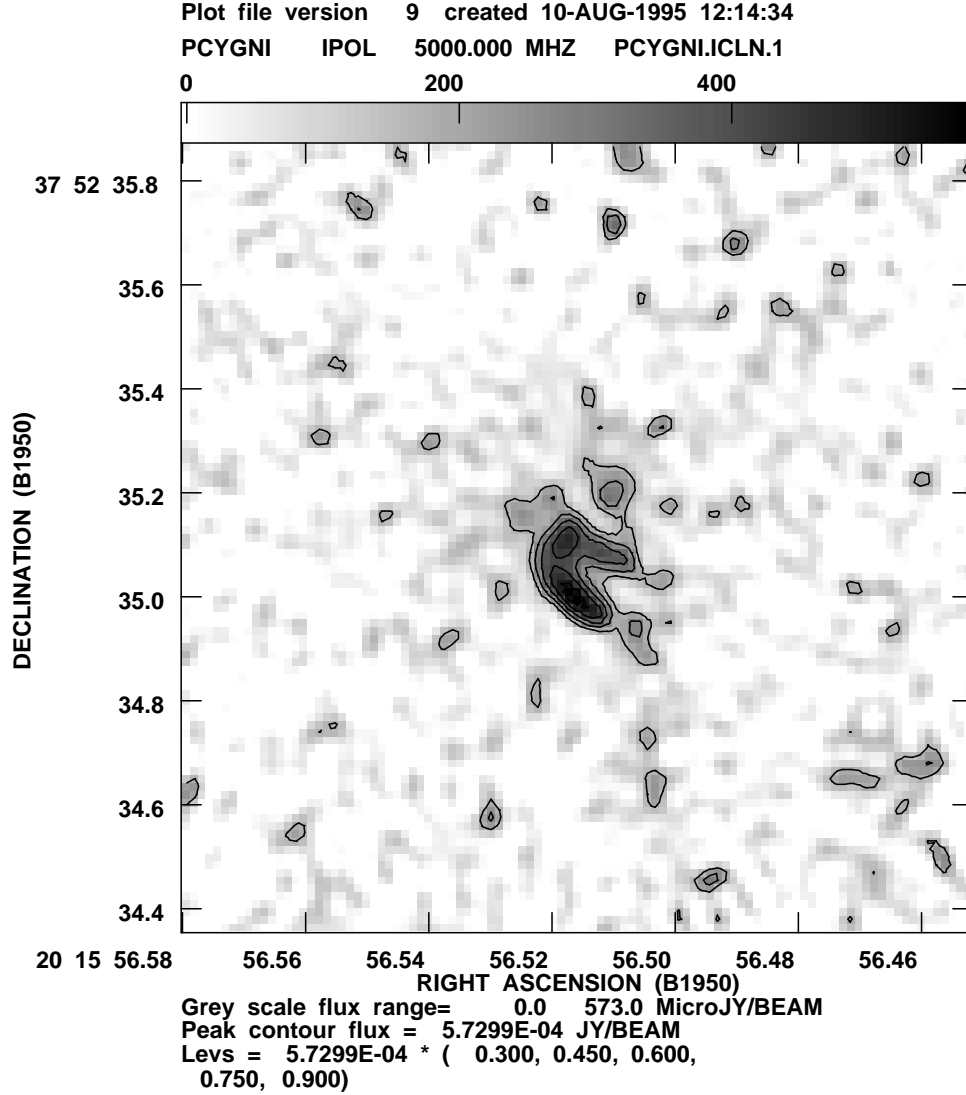


Figure 3. 6-cm MERLIN image of P Cyg from 1992 August 04. The synthesized beam is an ellipse of FWHM 48×51 mas².

Table 1. Parameters of P Cyg from MERLIN images.

Parameter	1992 June 24	1992 August 04
S_ν [mJy]	$4.76^{(+0.46)}_{(-0.20)}$	$3.80^{(+0.10)}_{(-0.29)}$
rms noise [mJy beam ⁻¹]	0.105	0.099
Beamsize [mas]	51×48	51×48
Size of emitting region [arcsec]	0.2×0.15	0.17×0.17

Table 2. VLA configuration summary.

	A	B	C	D
Longest baseline [km]	36.4	11.4	3.4	1.03
Shortest baseline [km]	0.68	0.21	0.073	0.033
θ_b (6 cm) [arcsec]	0.4	1.2	3.9	14
θ_b (2 cm) [arcsec]	0.14	0.4	1.2	3.9
θ_{\max} (6 cm) [arcsec]	10	36	120	300
θ_{\max} (2 cm) [arcsec]	4	12	40	90

variability, with the possible effects of resolving the radio source removed, and secondly we would like to use the very long total integration time to synthesize a very deep image, which because it uses all possible VLA configurations will be sensitive to flux on all size-scales. These two goals are inextricably linked, since removal of baseline effects requires a knowledge of the source extension, while in order to make a high-sensitivity map it is necessary to obtain good amplitude and phase solutions to each individual data set, and this requires compensation for any source variability. We therefore undertook a considerable amount of analysis of these data in order to generate the final products.

Combining all the observations would not make sense if the source structure varied as well as the total flux. This could happen, for instance, if a change of mass-loss rate manifested itself as a change in source brightness which slowly propagated out through the source like a ripple on a pond. Examination of the visibility curves for all the observations suggests that there is not much structural change: basically the entire visibility curve is scaled by some factor. This is consistent with the MERLIN data, which show that, although the appearance of the nebula has changed on a 40-d time-scale, the visibility curve does not change very much because

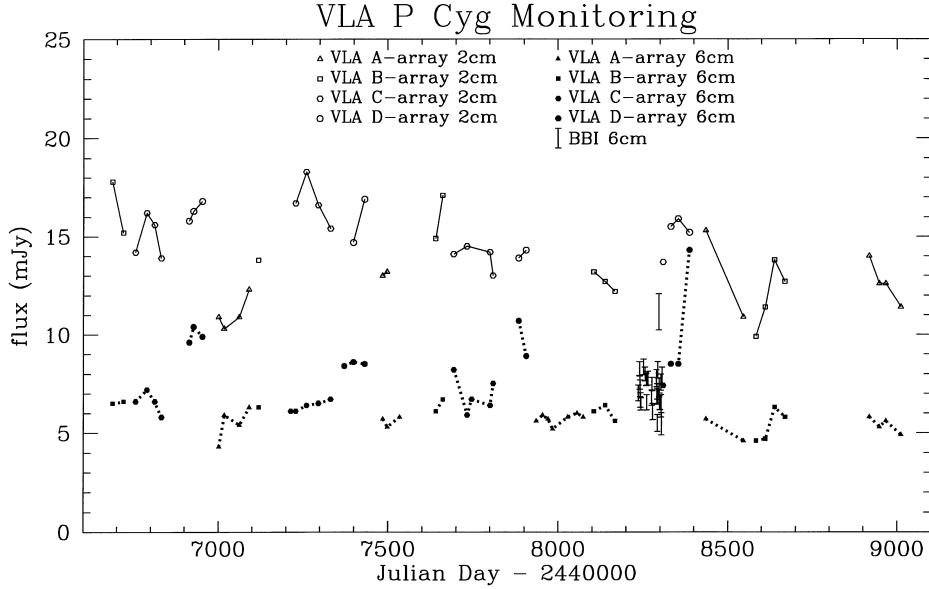


Figure 4. VLA observations of P Cyg from 1986 to 1992 at 2 and 6 cm. The fluxes have not been adjusted to allow for the different array configurations, and the effects of changing between configurations are very obvious from the roughly 15-month cycle seen in the data.

the size-scale of the brightest structures does not change much. This being the case, we can meaningfully combine all the data.

There is some ambiguity in the phase solution for such combined data, in the sense that zero phase may move slightly from one observation to another. The effect of this would be to degrade the spatial resolution of the data slightly. This is a particular problem for the A and B array configurations. Therefore we first reran the phase calibration for each data set, in order to move P Cyg artificially to the phase centre of every data set. Then all of the individual data sets were combined, and images made. The resulting images reveal considerable extended structure. Because of our concern that this kind of low surface brightness extended structure might be artificially generated owing to imperfect cleaning of data that included many observations of a point source with slightly different amplitudes, we now ran an amplitude self-calibration for combined data sets for each array configuration, to force all the observations on to the same flux scale and remove the effects of variability. After recombining the four data sets (one for each array configuration), we were now able to transform the recalibrated, combined uv data set into images. We found that these agreed very closely with the images made before the uv amplitude solutions were renormalized, strongly confirming that the extended structure we have detected is real, and not an artefact of poor calibration. Finally, to recalibrate the fluxes, we generated a combined ‘mean’ visibility curve for the single, combined uv data set. We then determined for each observation the scaling factor that allowed the individual visibility curve to fit the mean visibility curve best. This gave us relative photometry for each date. This was used in concert with the mean total flux, determined by integrating the flux in the images out to a radius at which the nebula became undetectable, to determine the absolute photometry. The results are presented in Fig. 6. Using the mean visibility curve, we have estimated that the BBI should have detected only about 82 per cent of the total nebular flux detected by the VLA. We have therefore scaled the BBI fluxes accordingly, and show these also in Fig. 6: they show reasonable agreement with the typical VLA fluxes. In particular, the last BBI observation was made within a few hours of one of the VLA observations, and the two observations, after these final stages

of calibration, agree to within about 0.1 mJy. For some of the observations plotted in Fig. 4, the visibility curves at one or both wavelengths showed excessive noise, suggesting poor calibration (most often at 2 cm owing to poor sky conditions), and we have not recalibrated these data, nor displayed them in Fig. 6. Using our visibility curves, we find mean total radio fluxes as listed in Table 3.

The 2- and 6-cm light curves for P Cyg show significant variability, but only minimal correlation. The maximum peak-to-trough amplitude at 2 cm is 49 per cent, compared with 65 per cent at 6 cm. Typical values are substantially smaller, and at 6 cm comparable to the level of variability seen with the BBI. This implies that long-term monitoring does not reveal behaviour significantly different from that observed in our much shorter term study with the BBI, or, put another way, that the variability is probably mostly occurring on a time-scale of a few days as determined from the BBI data. The 2- and 6-cm fluxes sample different regions in the P Cyg envelope, and so, if the variability has a fairly short time-scale (a month or less), the time-scale for propagation of a variation outward through the nebula is significant compared with the time-scale for the variability itself, and thus the 2- and 6-cm variations can be either poorly correlated or entirely uncorrelated. Tests (using nearby sources detected in the VLA data) suggest that our technique for estimating relative photometry from the visibility curves is accurate to typically ± 6 per cent, so that most of the variability apparent in Fig. 6 is real.

5 THE DEEPEST RADIO IMAGES OF P CYGNI

Using the combined uv data set generated as described in the previous section, we have generated a visibility curve which we present as Fig. 7. For a source which is circularly symmetric on a large scale (even if it is inhomogeneous on smaller scales), the imaginary component of the visibility should be zero. We see in Fig. 7 that indeed the imaginary visibility at 2 and 6 cm is zero within the noise, so that on a large scale the nebula is circularly symmetric. The real part of the visibility is then equal to the total visibility amplitude. We see that the visibility curve is somewhat complicated, but suggests that the radio source is extended out to a

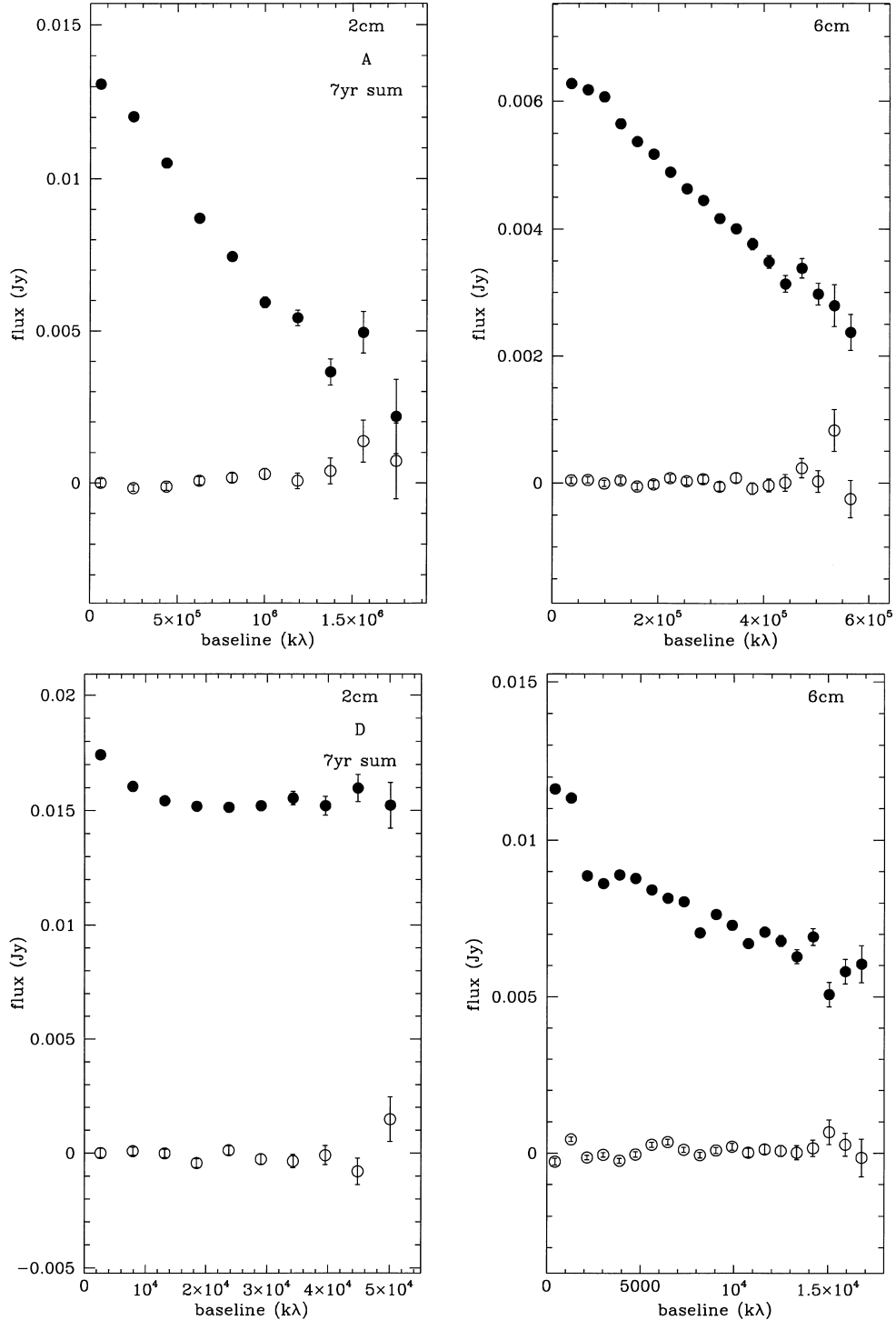


Figure 5. VLA visibility curves for P Cygni using A and D array data combined over the entire seven-year monitoring campaign at 2 and 6 cm. It is easy to see that even in D array P Cygni is resolved. Filled and open circles correspond to the real and imaginary parts of the visibility respectively.

radius of at least 2000λ at 6 cm, which corresponds to about an arcminute. The same result derives from the 2-cm visibility curve.

Given these visibility data, it is clearly worthwhile attempting to make deep images. We have therefore done this for each wavelength, using a variety of parameters. In making these, we have used natural weighting for the visibilities, which yields the best possible S/N at the expense of slightly inferior spatial resolution (as

compared with uniform weighting). In Fig. 8 we show a 6-cm image made with 0.2-arcsec pixels, with a slight taper applied to the visibility data to smooth the image and improve the S/N. The effective beam is circular with a diameter of about 2 arcsec.

Considerable structure is visible surrounding the central compact stellar wind source, which is slightly asymmetric. The structure is either filamentary or blobby, the resolution of the image being

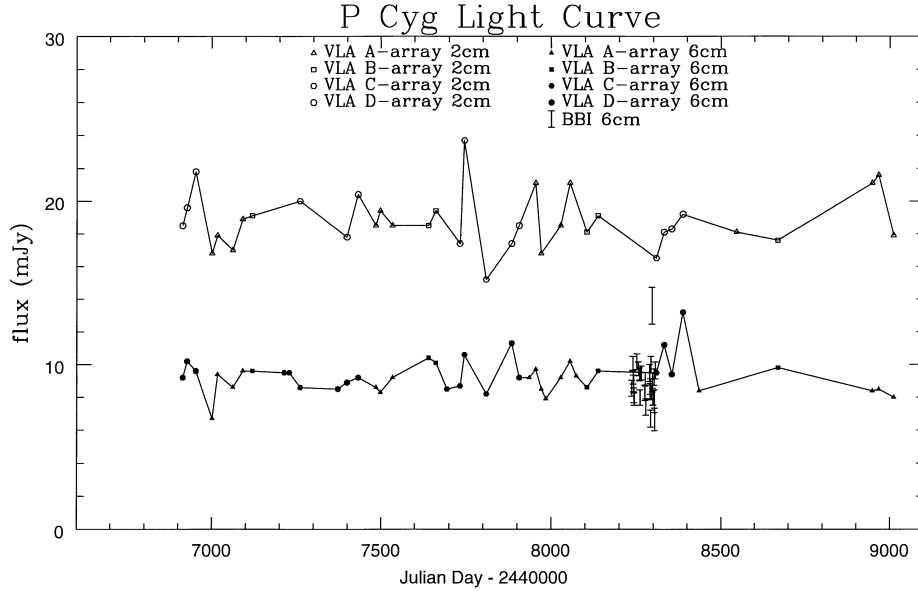


Figure 6. VLA observations of P Cyg from 1986 to 1992 at 2 and 6 cm. The fluxes have been adjusted to allow for the different array configurations, and so the variability seen in this figure should be real.

Table 3. Total radio fluxes for P Cyg.

Facility	Wavelength [cm]	Flux [mJy]
BBI	6	8.6 ± 0.5
VLA	6	10 ± 1
VLA	2	17 ± 1

insufficient to distinguish. There appears to be a sharp edge to this structure at a radius of around 8–9 arcsec, beyond which the surface brightness drops below the noise threshold of the image. Similar structure has recently been reported by Barlow et al. (1994)

who obtained optical coronagraph images, and in Fig. 9 we present these optical data as contour overlays on top of the 6-cm image, which has in this case been degraded to a 0.255-arcsec pixel size to match the optical image. Whilst there is not perfect correspondence, it is clear that much of the structure in the radio image is reproduced in the optical image, and vice versa. It therefore seems probable that we are seeing the same material in both optical and radio images. At 2 cm no extended structure could be seen brighter than 2σ .

Next we employed a larger pixel size, 0.8 arcsec, and made images at both 2 and 6 cm with a much stronger taper applied to degrade the beam to a circle of diameter 13 arcsec. Increasing the taper degrades the spatial resolution of the resulting images, but improves the S/N. We display the two images, plus an overlay of the two, in Figs 10, 11 and 12.

VLA 7yr Composite Visibility Curves

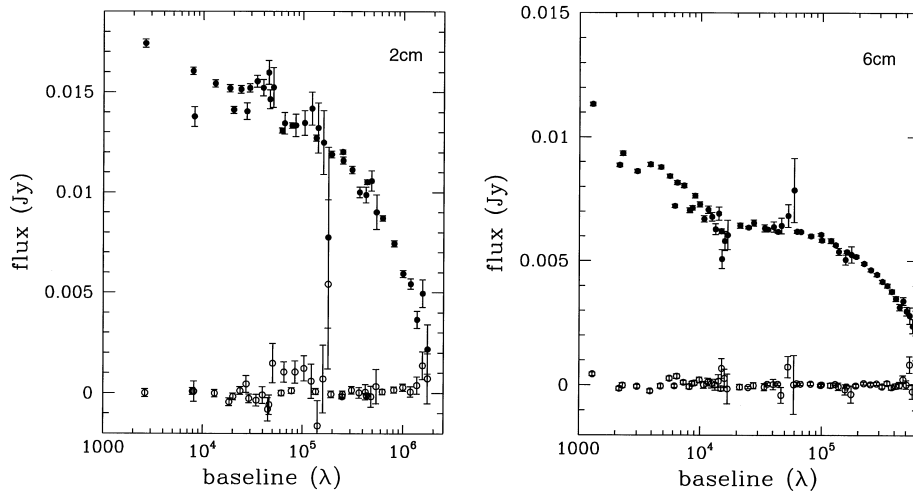


Figure 7. Combined VLA visibility curve for P Cyg, using all data from all array configurations. Visibility is seen to increase down to the shortest available baselines, indicating a very extended structure. Filled and open circles represent the real and imaginary parts of the visibility respectively.

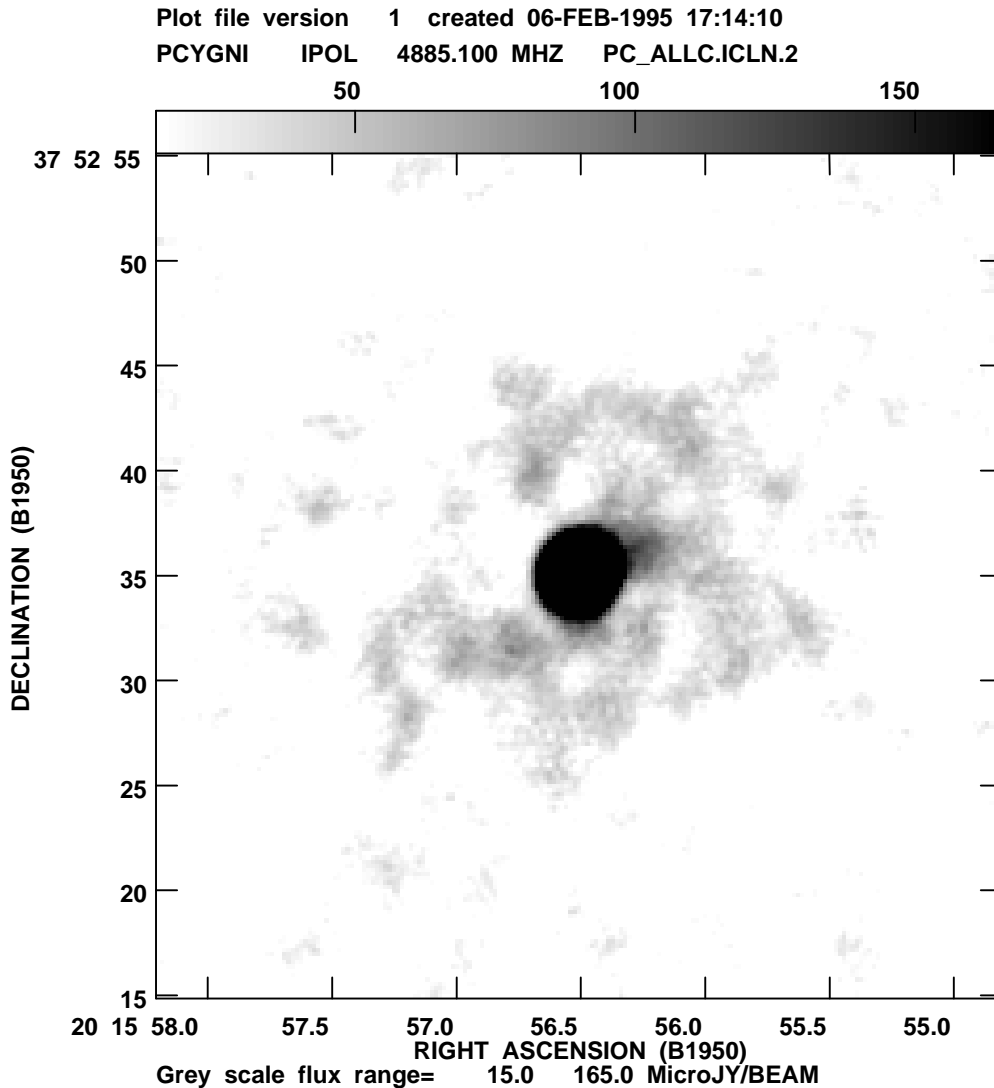


Figure 8. VLA 6-cm image of P Cyg, with 0.2-arcsec pixels and a 2-arcsec beam. Considerable structure is seen in an inner nebula out to about 10-arcsec radius.

Again the S/N is worse in the 2-cm image, so that the structure is much clearer in the 6-cm image, but the overlay demonstrates the remarkable degree of correspondence between the two images. If the extended structure seen were really due to poor cleaning of the image or some bad calibration effect, quite different results should be expected from the two images which use entirely different data sets with different baseline combinations. Again, Barlow et al. (1994) presented optical coronagraphic images which revealed structure extended on the scale of these images, so we present overlays of the Barlow et al. optical images with our 6-cm image as Fig. 13. As with the previous resolution, we see much the same material emitting in both the radio and the optical. Particularly prominent in both the radio and optical images are a broken arc of emission at a radius of about 40–45 arcsec from the west-north-west around to the north-east, and some filamentary material at about 20–25 arcsec in a variety of directions. Closer to the star than this the optical images are saturated. In the southernmost portion of the optical image there appears to be a significant drop in sensitivity, with the result that there may well be nebulosity present here that is not detected in the image.

Lastly, we used 3-arcsec pixels and a heavy taper, resulting in 25-arcsec resolution, to make the 2- and 6-cm images presented as

Figs 14, 15 and 16. These reveal a wealth of structure in the environment around P Cyg, which is probably to be expected in an OB association. We see that P Cyg's radio nebula more or less surrounds it, to a distance of just over 1 arcmin, at which point the surface brightness drops rapidly into the noise. The nebula is brightest in an arc which runs from the north-west around to the north-east, and corresponds closely to the structure seen in 20-cm images by Baars & Wendker (1987). A strand of relatively bright radio nebulosity extends almost 2 arcmin to the east-north-east from a position about 2 arcmin north-east of P Cyg. The end of this strand closest to P Cyg almost coincides with an optically visible star (see Fig. 13). A considerable amount of radio structure in this region of the sky may correspond to interstellar gas heated by the thronging young, hot stars here. We see four unresolved radio sources in Fig. 16, each of which has also been detected by Baars & Wendker (1987) at 20 cm, and which are probably stars in the IC 4996 cluster.

At 6 cm, we find that about 40 per cent of the total VLA flux arises in the compact central source, which is a few tenths of an arcsecond in diameter. About another 40 per cent or so of the flux arises in the 10-arcsec nebula, and the remainder in the outer,

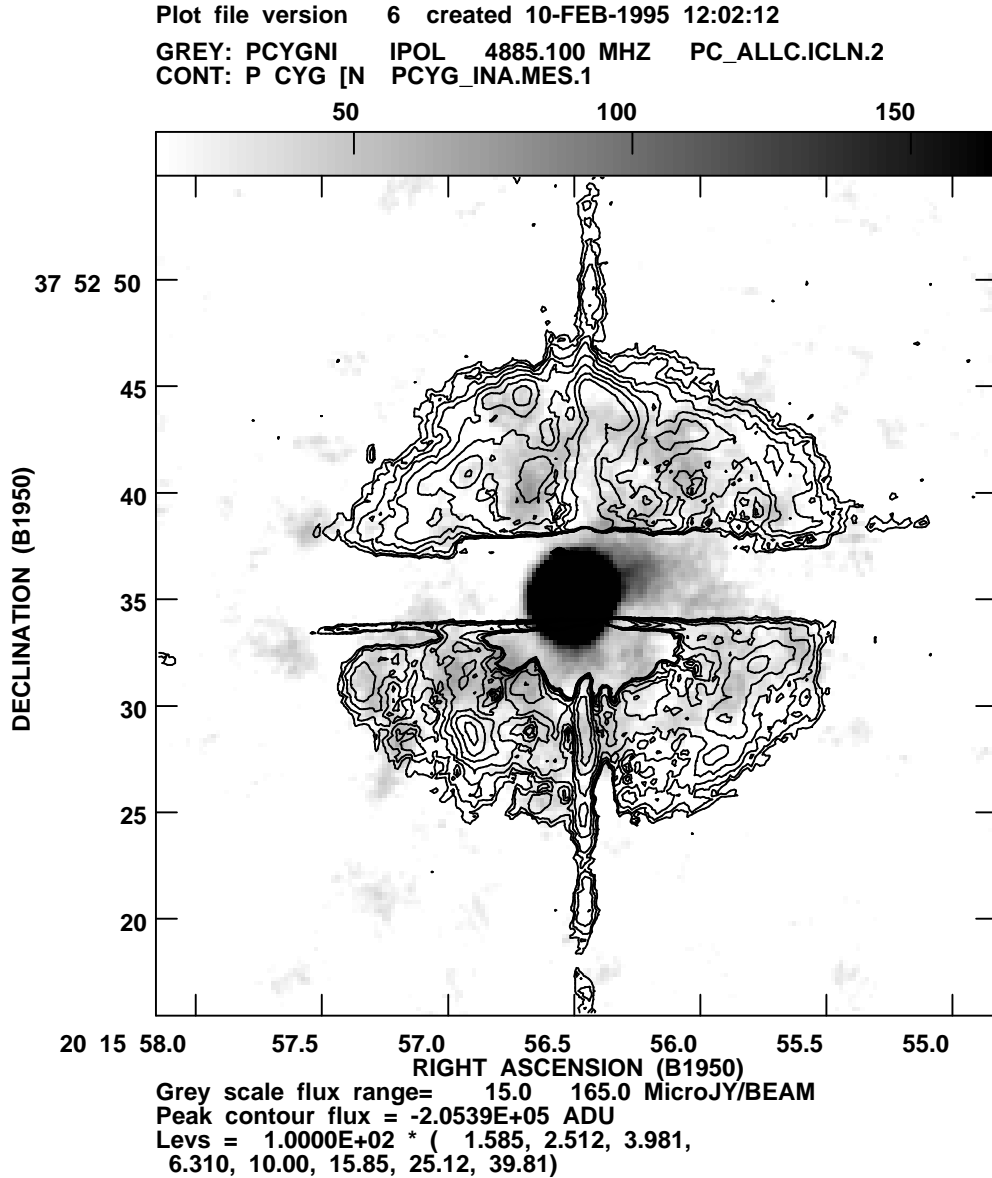


Figure 9. VLA 6-cm image of P Cyg, with 0.255-arcsec pixels and a 2-arcsec beam, with the optical image of Barlow et al. (1994) overlaid in contours. Much of the structure in the two images coincides. Note that the optical image was taken via a bar-coronagraph. The north–south spike in the optical image is part of the telescope diffraction pattern.

arcmin-scale nebula. The emission from the nebula is clearly thermal. In the 10-arcsec nebula, the spectral index (derived from the 2- and 6-cm images alone) over much of the nebulosity is about 0.8, consistent with at least partially optically thick free–free emission. In the outer nebula, the spectral index is much lower, in general fairly close to zero, indicative of optically thin free–free emission.

6 A MODEL FOR THE RADIO EMISSION

The radio and infrared emission from P Cyg has been modelled by a number of previous authors. However, most previous work has either used a very simple isothermal wind model (e.g. Barlow & Cohen 1977), or treated only a part of the wavelength range over which the wind significantly affects the spectral energy distribution (e.g. White & Becker 1982; Waters & Wesselius 1986). Deacon

(1991) and Deacon & Barlow (1991) modelled the radio and IR emission from P Cyg using the Drew (1985) temperature distribution, but had none of the observed spatial information that we now have. In this section we will present a model which can account reasonably consistently for all the radio observations that we have described in this paper, as well as for previously published observations of P Cyg throughout the IR.

The model used is essentially that described by Skinner et al. (1997a) for the free–free excess of the M supergiant α Ori. Briefly, the circumstellar environment of P Cyg is assumed to be spherically symmetric, and the geometry used is the same as that of the model of Waters & Wesselius (1986). An electron temperature distribution is read into the model (we began with that presented by Drew 1985), and adjusted as required to obtain a good fit to the data. The velocity law for the stellar wind is assumed to follow the behaviour used by Waters & Wesselius, which is to say the wind velocity is assumed to

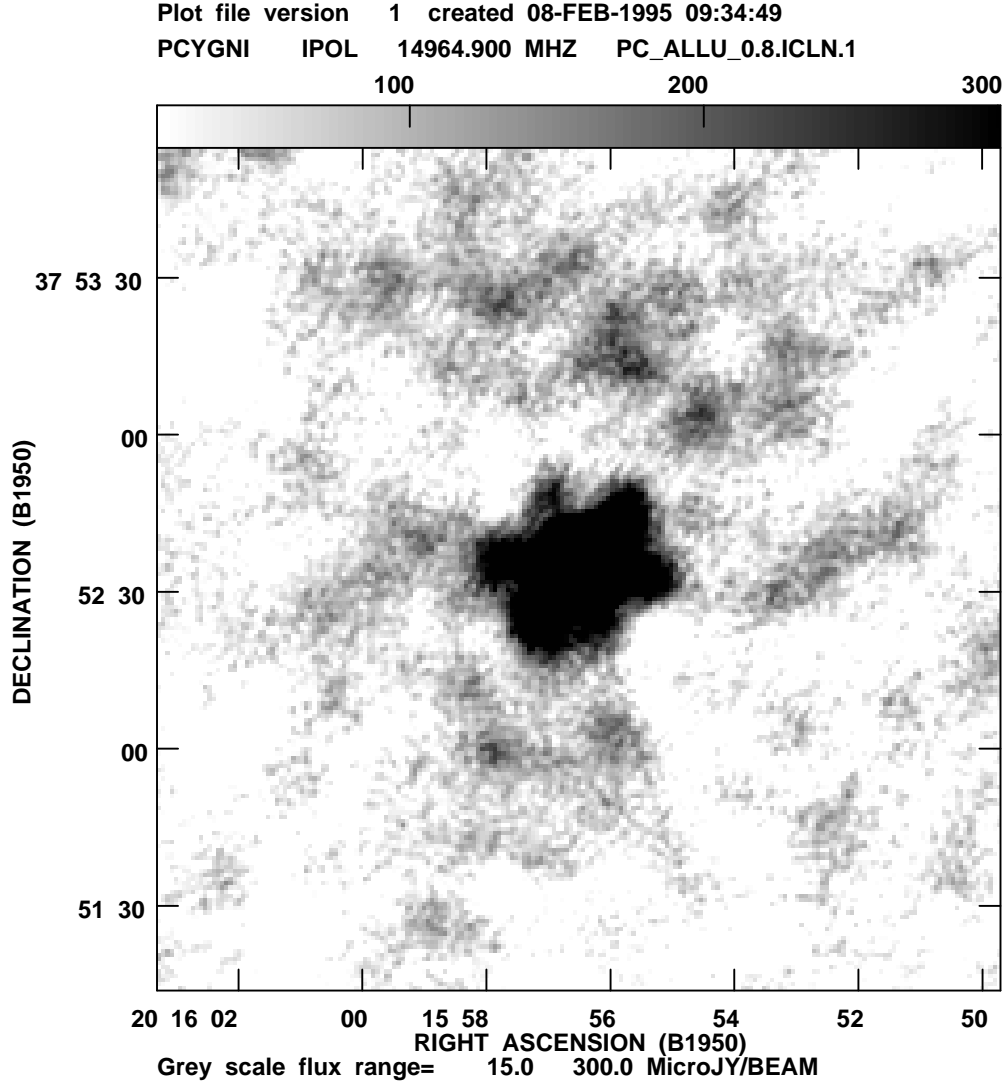


Figure 10. VLA 2-cm image of P Cyg, with 0.8-arcsec pixels and a 13-arcsec beam.

increase linearly from an initial value v_0 to 90 per cent of its terminal value by some radial distance X , after which the wind speed is assumed to increase asymptotically towards its terminal value. The value X is left as a free parameter to be determined by modelling (Waters & Wesselius determined a value of 15 stellar radii using their model of the IR emission). Other velocity laws can provide a good fit to the IR energy distribution, and it is not possible to determine which is best, so we have simply used the above law for convenience. This will be discussed further later. The electron density is determined as a function of radius from the stellar mass-loss rate and the velocity law described above. Previously published estimates of P Cyg's mass-loss rate mostly lie in the range $1-3 \times 10^{-5} M_{\odot} \text{ yr}^{-1}$, and we have found that mass-loss rates close to this range are needed to fit the observations. Waters & Wesselius (1986) appear only to have modelled the wind out to distances of a few hundred stellar radii from the central star, which is the region in which all the IR emission arises. They therefore only determined Gaunt factors for wind electron temperatures above about 10 000 K. We have used the techniques described fully by Skinner et al. (1997a) to determine the wavelength-dependent Gaunt factors for any electron temperature and density, and we consider the wind out

to a distance of approximately 1 pc from the star. Although this may seem rather a large distance, Barlow et al. (1994) observed optical line nebulosity as far as about 0.5 pc from the star, indicating that there is certainly material at this distance that is warm and dense enough to be emitting in optical forbidden lines. The observations (both radio and optical) show that the P Cyg nebula is certainly rather clumpy. Our model is spherically symmetric, and so can only be treated as an estimate of the average conditions through the nebula. The fit of the model to the data will show that this approach is reasonable.

With a constant mass-loss rate of approximately $10^{-5} M_{\odot} \text{ yr}^{-1}$, we find that we are able approximately to fit the IR spectral energy distribution, the dimensions of the 6-cm emitting region as determined from the MERLIN image, and the 2-, 6- and 20-cm fluxes of the hot, inner core of the wind. However, we do not obtain a good fit to the visibility curves at short baselines, where the visibility rises significantly, indicating the presence of more extended radio emission. As a result, such a model does not fit the total radio fluxes well.

By adopting a time-variable mass-loss rate, we are able to obtain a much better fit to the data. In Fig. 17 we show the fit to the spectral energy distribution obtained with such a model. (Note that the

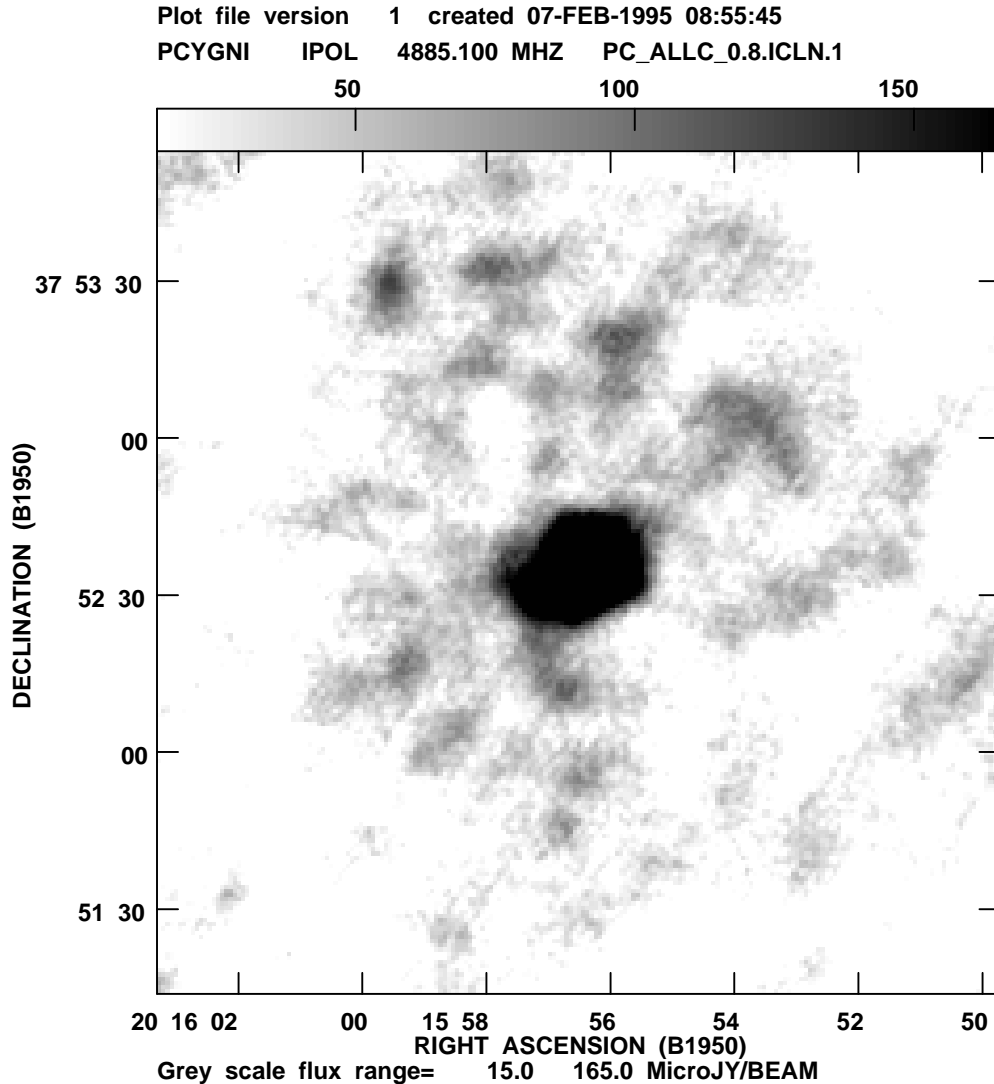


Figure 11. VLA 6-cm image of P Cyg, with 0.8-arcsec pixels and a 13-arcsec beam.

observations presented in this figure were obtained at many different epochs, which may introduce some scatter owing to source variability.) The distributions of electron density and temperature that were required to obtain this fit are shown in Fig. 18. The resulting fits to the visibility curves at 2 and 6 cm are shown in Fig. 19, and the fit of this model to the azimuthally averaged radial surface brightness profile is shown in Fig. 20. The fit to the visibility data is imperfect, but it is likely that the poor fit at long baselines is because the nebula is highly inhomogeneous, adding more power to high spatial frequencies than our spherically symmetric model can predict. Finally, the mass-loss rate as a function of time implied by this model is shown in Fig. 21. The rest of the parameters used to generate this model are listed in Table 4.

It should be noted that this model has been entirely empirically determined – the parameters or distributions obtained from it are not obtained from a physical model of a nebula, but purely from the requirement that the observations of this source must be fitted. The combination of electron temperature and density is fairly well constrained in the ‘core’ of the radio nebula (at radii of no more than an arcsecond), by the combination of spectral energy distribution and visibility curves. Using too high an electron temperature

causes too low an optical depth and thus too much flux and too shallow a spectral slope. Too low an electron temperature results in too large an optical depth, and hence the flux becomes weighted too heavily toward short baselines in the visibility curve, too little flux emerges overall, and the spectral slope becomes too steep. Electron densities similarly affect the spectral energy distribution and visibility curves, and with two complete visibility curves as well as a spectral energy distribution covering a very wide waveband, we are able to constrain the density and temperature distributions quite strongly. Waters & Wesselius (1986) used a velocity law for the wind which approached terminal velocity close to 15 stellar radii, while Barlow & Cohen used a law reaching 90 per cent of terminal velocity at 40 stellar radii. In order to fit both the spectral energy distribution (SED) and the visibility functions we needed to adopt a velocity law of the type used by Waters & Wesselius, but which reaches 90 per cent of terminal velocity at 80 stellar radii. With this ‘90 per cent’ radius set either as low as 50 stellar radii or as high as 100 stellar radii, we are unable to fit both the entire SED and the visibility curves. The initial velocity, v_0 , was found to yield the best fit when set to 20 km s^{-1} , in agreement with the results of Waters & Wesselius. We note that a variety of evidence suggests that the

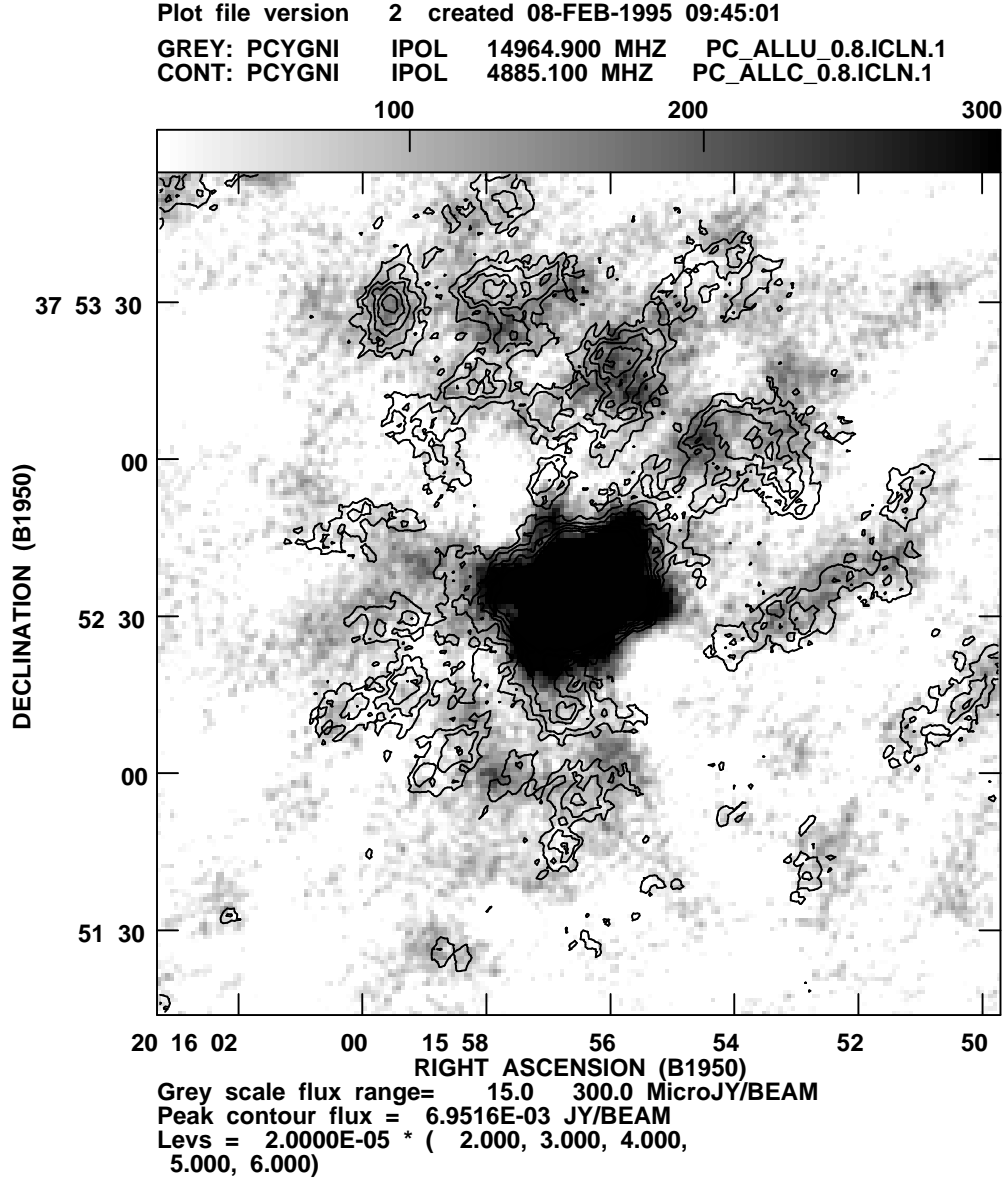


Figure 12. VLA 2- and 6-cm images of P Cyg, with 0.8-arcsec pixels and 13-arcsec beams. The 2-cm image is in grey-scale, with the 6-cm image overlaid in contours.

electron scattering optical depth is significant in the innermost portion of the P Cyg wind, and our code does not include electron scattering. As a result the velocity law adopted by us for the inner portion of the wind must be viewed with caution. Our other conclusions should be unaffected by electron scattering. The IR and submillimetre excess continuum arises in the accelerating part of the outflow, while the millimetre and radio part arises in the region external to this ‘90 per cent’ radius, and thus obtains a different spectral slope (see Fig. 17). We note that the electron temperature structure in our model is very similar to that determined theoretically by Drew (1985). In the innermost portion, closer to the star than 5 stellar radii, the electron temperature distribution in our model falls rapidly with increasing radius, and is very close to that calculated by Drew. Further out, in the 5 to 50 stellar radii region, the temperature in our model actually falls a little more slowly than calculated by Drew, and the temperature in our model at 50 stellar radii is 11 000 K compared with only 9000 K

in Drew’s results. None the less, in this inner region our results basically lend support to the work of Drew (1985), which should be consulted for the physical basis of the temperature structure. In our model the temperature only reaches 10 000 K at about 10^4 stellar radii, beyond which we allow it to fall fairly rapidly. If we allow the temperature to fall more rapidly inside this inner nebular region, then in order to fit the radial profile of the 6-cm emission we have to adopt a density distribution that corresponds to a mass-loss rate slowly increasing with radius (and hence look-back time). The drop in electron temperature in our model at about 10^4 stellar radii coincides with the mass-loss outburst in the model, and could result from increased radiative cooling as a result of line emission at the increased density. The expansion velocity derived by Barlow et al. (1994) for the 11 arcsec radius optical nebula was only 110 km s^{-1} , while we have been assuming that the current velocity of 206 km s^{-1} applies throughout the nebula. A 6-arcsec nebula which may be present in the data of Barlow et al. was suggested

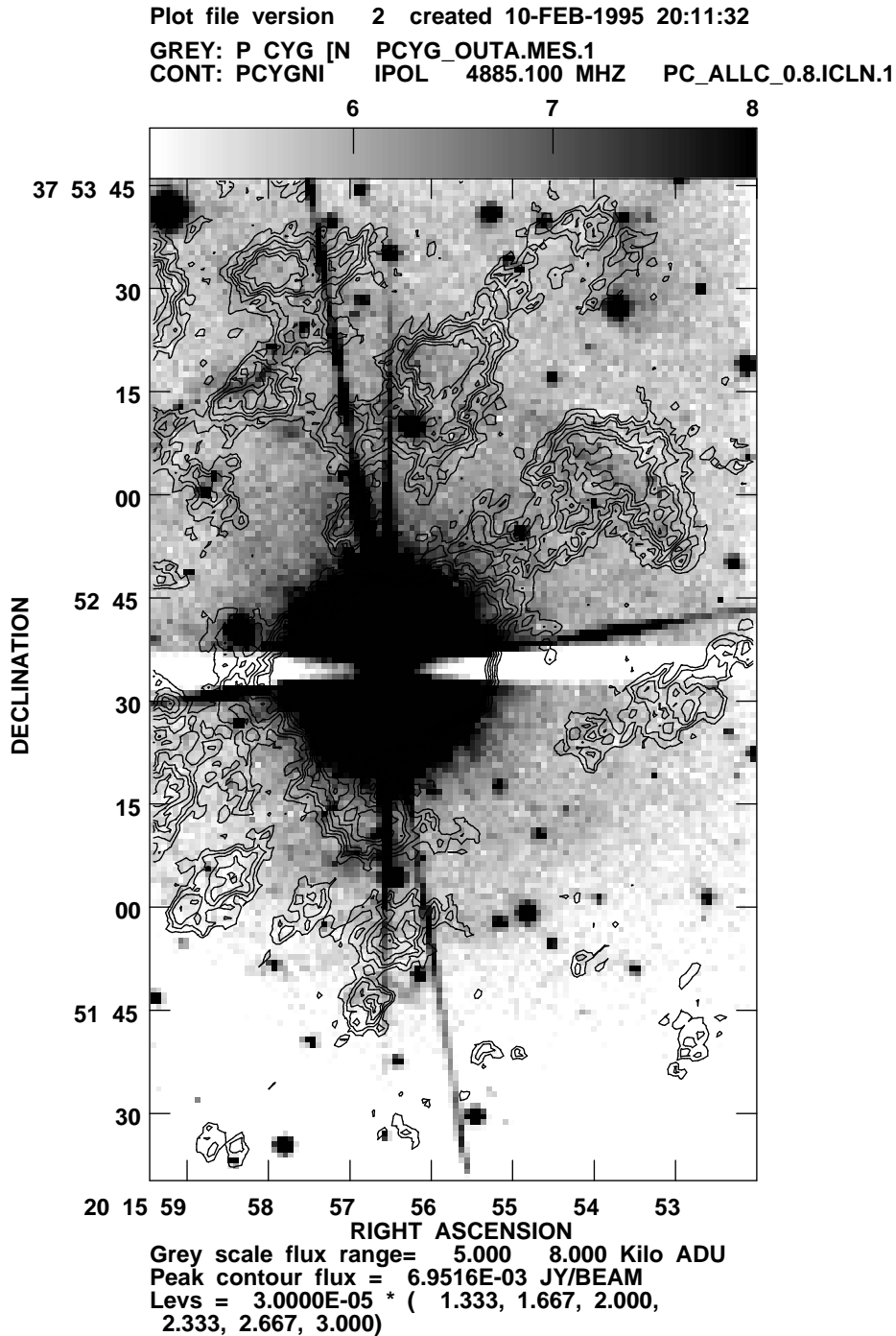


Figure 13. VLA 6-cm image of P Cyg (contours) with 0.8-arcsec pixels and a 13-arcsec beam, overlaid on an optical image from Barlow et al. (1994) in grey-scale. Note that there is a significant decrease in sensitivity in the lower portion of the optical image, so that some nebulosity may be present but not detected here.

by them to correspond, at an expansion velocity of 110 km s^{-1} , to the AD 1600 outburst. The lower velocity in this region would correspond to a higher electron density for the same mass-loss rate. At 10^4 stellar radii, in order for the [S II] emission to yield a roughly solar sulphur abundance, as would be expected for P Cyg (e.g. Johnson et al. 1992), the electron temperature would have to be close to 6000 K, somewhat lower than our model has used. The combination of lower expansion velocity and lower temperature than our model uses, which is observed in this region, is probably more or less consistent with our model (the lower temperature

would decrease the nebular emission, and the lower expansion velocity increase it), but requires a degree of extra sophistication in the model which we regard as not yet justified by the observations.

At larger radial distances from the star, the temperature and density become less well constrained. We find that we require an elevated mass-loss rate in the past (Figs 18 and 21), with two episodes of high mass-loss rate. The most recent that we find occurred roughly 400 yr ago, which would coincide very closely with the optically visible ‘outburst’ of P Cyg in AD 1600. We find

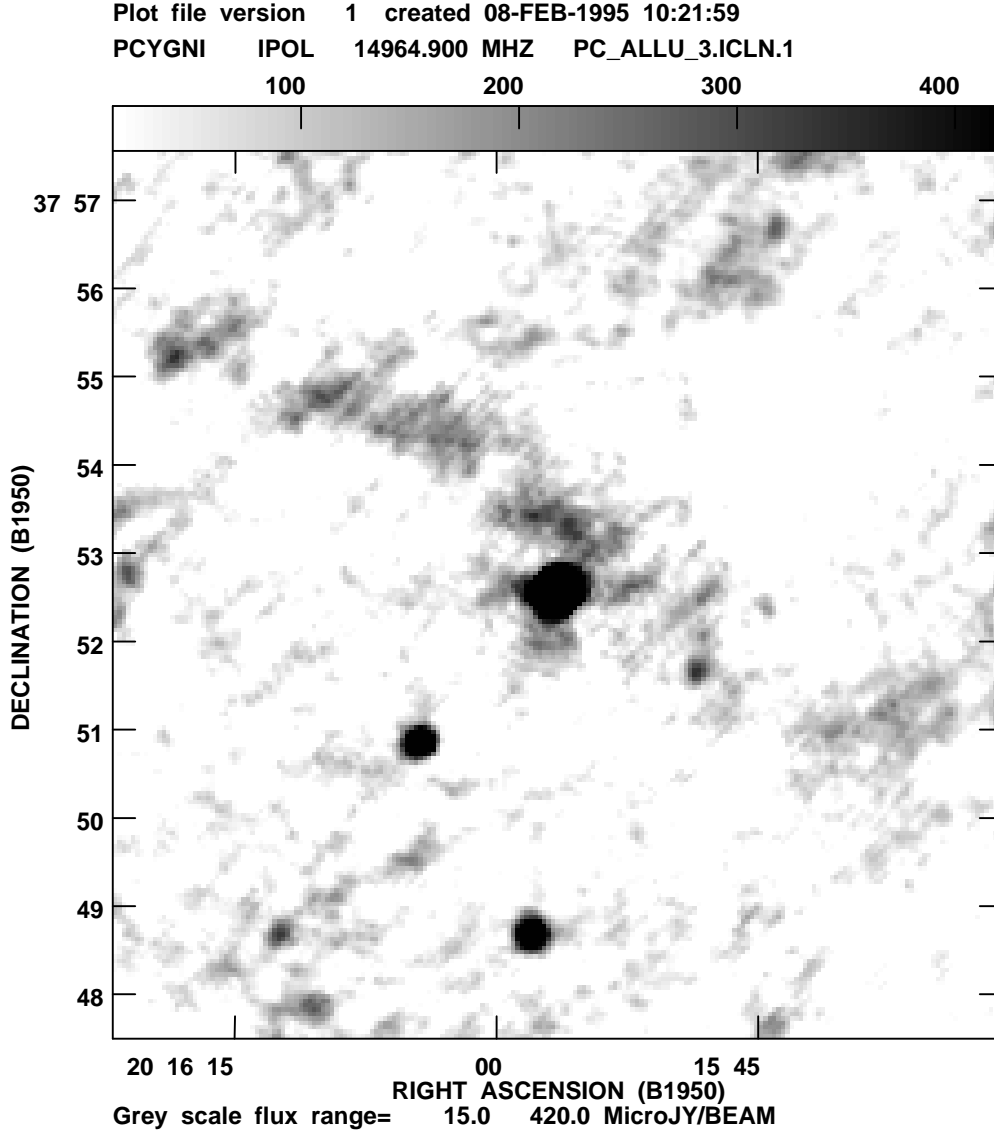


Figure 14. VLA 2-cm image of P Cyg, with 3-arcsec pixels and a 25-arcsec beam.

that with a mass-loss rate during this episode of order $5 \times 10^{-5} M_{\odot} \text{ yr}^{-1}$ we are able to fit quite nicely the extended emission in the inner (10-arcsec radius) nebula. We are able to fit the observations with a single outburst of a duration of about a century, but a good fit to the data could also be obtained with a pair of outbursts (P Cyg was in fact observed to undergo two optical brightenings during the 17th Century). Further lower level mass-loss rate enhancements could also have occurred since then – our data do not allow us to discriminate small and short-duration events. The second event that we require occurred about 2000 yr ago. In order to fit the visibility data we require a mass-loss rate of about $1.4 \times 10^{-4} M_{\odot} \text{ yr}^{-1}$, with a duration of several hundred to a thousand years, but a better fit to the azimuthally averaged surface brightness profile would be obtained with a somewhat lower mass-loss rate. This mass-loss event could be entirely consistent with a foray into the red supergiant region, as was suggested by Waters & Wesselius (1986) to explain a supposed excess in the *IRAS* far-IR data (see later). Without any mass-loss rate increase we are unable to explain the increasing visibility with decreasing baseline, or any of the extended nebulosity seen in the VLA images. The electron tem-

perature distribution in the core follows much the same functional form as that predicted by Drew (1985), but is a little higher. Reducing the temperatures to exactly those presented by Drew results in a higher optical depth, and thus a significantly poorer fit to the visibility data at long baselines. In the inner and outer radio nebulae, there is associated optical forbidden line emission (Johnson et al. 1992; Barlow et al. 1994), which implies that the electron temperature is probably a few thousand degrees. We have used this to develop the model as indicated in Fig. 15, but, since the free-free emission is optically thin at distances from the star larger than 1000 stellar radii, the electron density and temperature distributions are degenerate. Between the two outbursts we have adopted a steady mass-loss rate which is double the current one. This provides a reasonable fit to the radial profile between the two ‘rings’ of emission. In practise our data are not adequate to distinguish between a constant, slightly elevated mass-loss rate during this period and a few slightly larger discrete mass-loss outbursts. Finally, we note that in deducing the mass-loss rates and look-back times listed above we have used a wind velocity of 206 km s^{-1} throughout the nebula. However, Barlow et al. (1994) deduced a

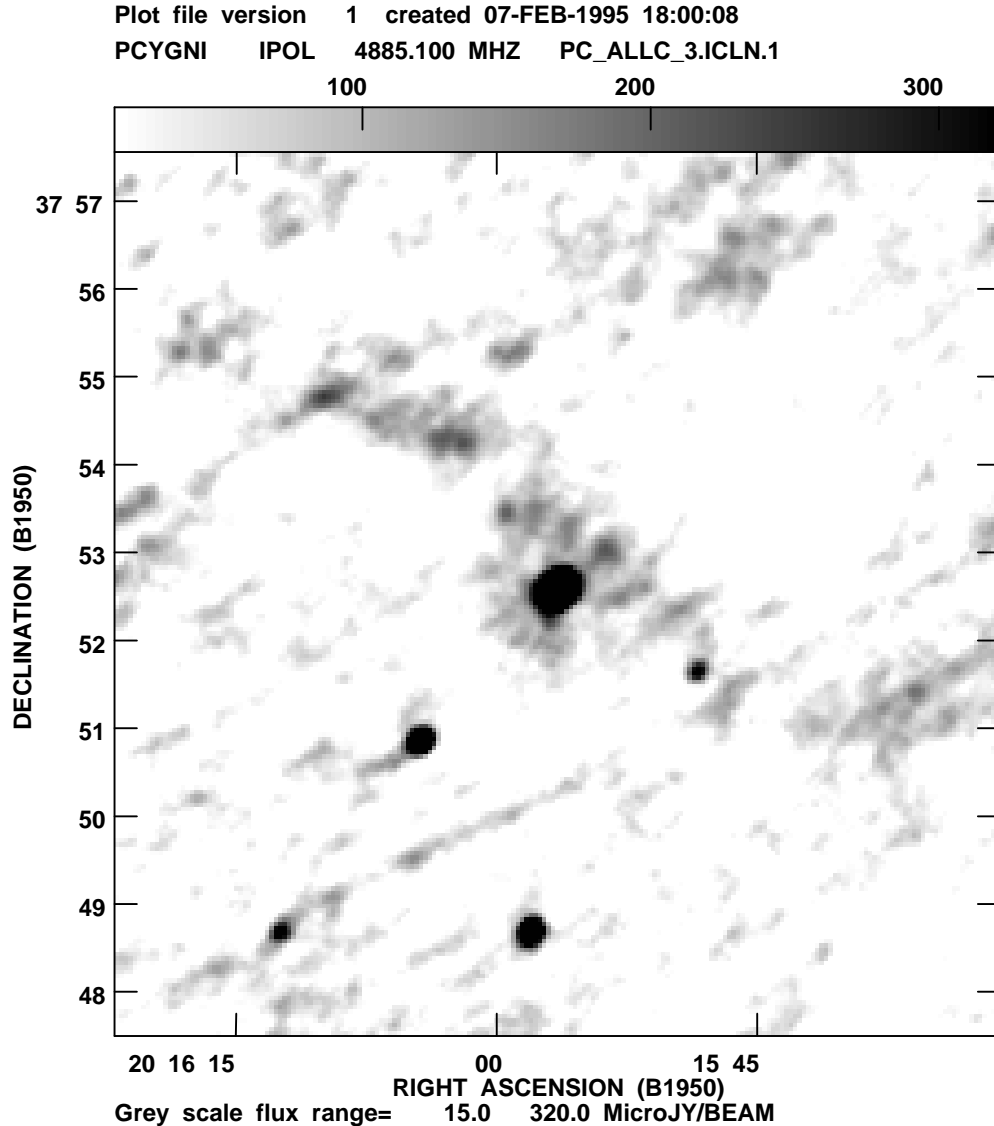


Figure 15. VLA 6-cm image of P Cyg, with 3-arcsec pixels and a 25-arcsec beam.

wind velocity of only 110 km s^{-1} for the 11 arcsec radius nebulosity. It is not clear whether the wind in this region is uniformly expanding at 110 km s^{-1} , or is mostly flowing at a higher velocity but bearing dense blobs moving more slowly, so there are some significant uncertainties in the values that we deduce.

7 DISCUSSION

The model that we have used is spherically symmetric and homogeneous. The radio images make it clear, however, that the nebula is actually highly inhomogeneous, either clumped or filamentary (or both). The effect of such inhomogeneity on the model will depend on the size-scale of the clumpiness. Very large-scale clumping of the material will allow us to ‘see’ into the wind to much greater depths at some radii, allowing the radio flux to rise at some wavelengths, and increasing the visibility at long baselines. Clumping on a much smaller scale will also increase the visibility at long baselines, but will have less effect overall on the total radio fluxes. The radius predicted by our model for the core (70 mas) is somewhat larger than that predicted by Barlow & Cohen (1977), and

reasonably consistent with that observed in the MERLIN images. The MERLIN data imply that the wind is probably clumped on a relatively small size-scale (less than 40 mas). Barlow et al. (1994) suggested that blobs seen in the optical nebula had been ejected during outbursts. Our MERLIN images, however, suggest that blobs are ejected in the ‘normal’ wind and are a regular part of the mass-loss process for this star.

A brightness temperature map of P Cygni (Skinner et al. 1997b) suggests that temperatures as high as 15 000 K may prevail in small regions in the core of the radio nebula. This is considerably higher than our model obtains at a few hundred stellar radii. On the other hand, the brightness temperature of much of the surrounding material is somewhat lower than our model would suggest. Clearly there is considerable inhomogeneity in the wind, and indeed it has been suggested by Barlow et al. (1994) that the wind may bear dense blobs moving at velocities somewhat lower than that of the ambient wind. They suggested that such blobs may generate a bow shock where the surrounding wind impacts them, leading to elevated temperatures and densities. In such a situation, the radio nebula can consist of a number of relatively hot, very dense emitting regions

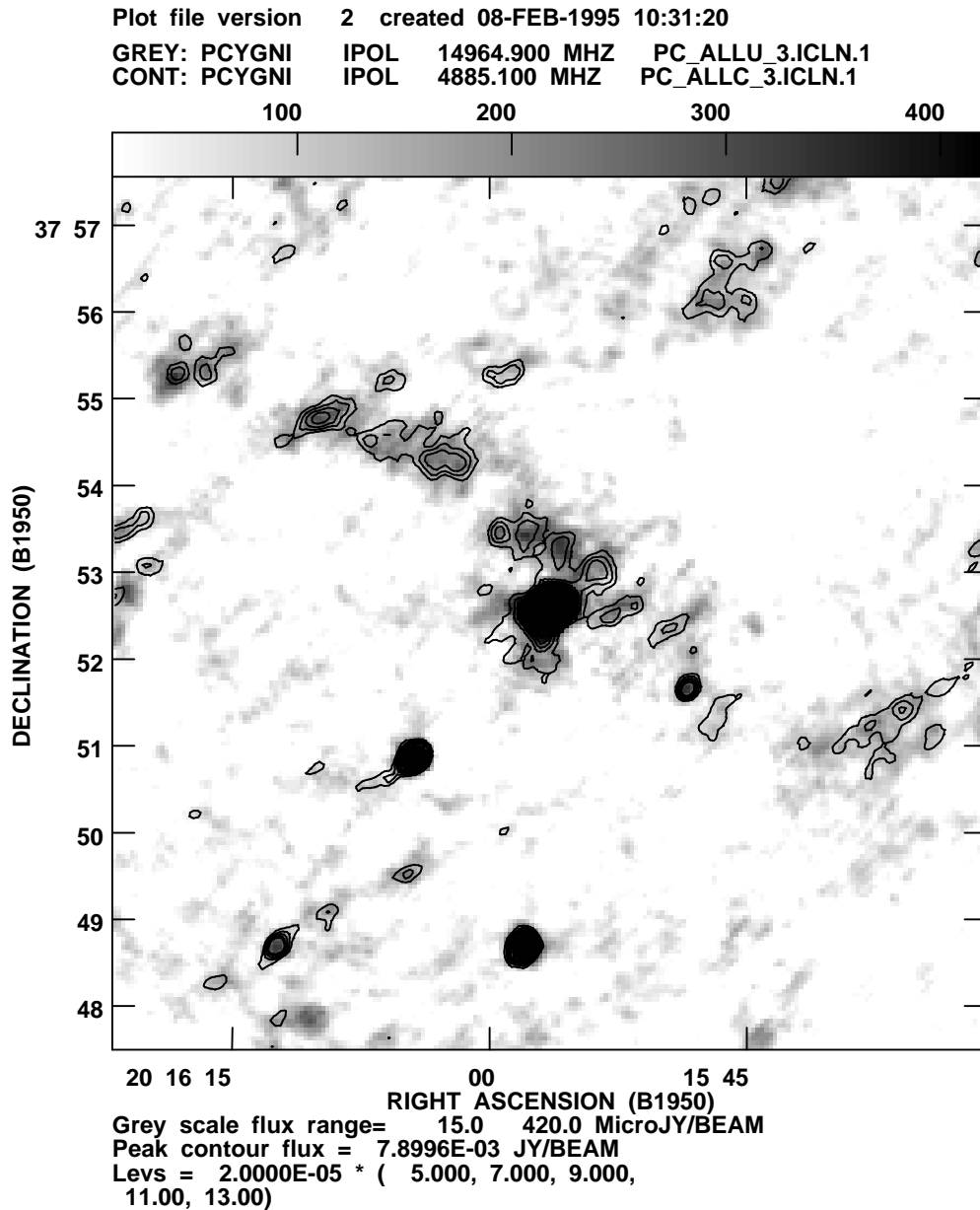


Figure 16. VLA 2- and 6-cm images of P Cyg, with 3-arcsec pixels and a 25-arcsec beam. The 2-cm image is presented in grey-scale, and the 6-cm image overlaid in contours.

surrounded by faster moving but much cooler wind. This would be quite consistent with all of our observations of this source with MERLIN and the VLA, and then our model simply represents a radial average of the highly inhomogeneous density and temperature structure and free-free emission.

The mass-loss history implied by our model is eventful, and the available observations dictate that the mass-loss rate cannot have been constant in the past. The two major events that we propose are absolutely required by the data, and are consistent with the radio and optical images now available, as well as with the available historical records. The event 2000 yr ago could have occurred at a time consistent with certain Biblical suggestions, although we suspect that our data are not precise enough to warrant submission to the Weekly World News yet. Waters & Wesselius have suggested that P Cyg may have undergone a red supergiant phase at the time of its AD 1600 outburst. They proposed this in order to explain the

unexpectedly large *IRAS* 60- and 100- μm fluxes in terms of dust emission. However, Deacon & Barlow (1991; also see Barlow et al. 1994 for a detailed discussion of the *IRAS* far-IR fluxes) suggest that inspection of the *IRAS* pointed observations of P Cyg implies that in fact the far-IR data are quite consistent with a free-free wind model, with no need to invoke dust emission. Given the uncertainties regarding these *IRAS* data, we have ignored the *IRAS* 100- μm observations in this paper. The mass-loss rates that we have determined during the two outbursts are entirely consistent with those of other known LBGs (e.g. Davidson et al. 1986) or red supergiants (e.g. Skinner & Whitmore 1988). Mass lost during an earlier red supergiant phase should have a significant dust content, since red supergiants with large mass-loss rates typically form large quantities of dust in their outflows (e.g. Skinner & Whitmore 1988). It seems that the *IRAS* data at 100 μm probably do not require the presence of any circumstellar dust, but the fluxes at 1.2 and 3.3 mm

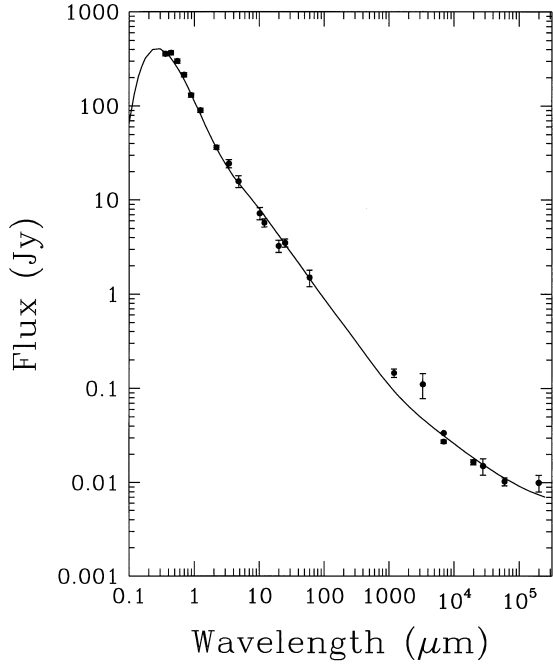


Figure 17. Spectral energy distribution of P Cyg, with the fit of our model (solid line). The observational data shown are from Abbott, Telesco & Wolff (1984), Waters & Wesselius (1986), *IRAS*, Altenhoff, Thum & Wendker (1994), Contreras et al. (1996) and Baars & Wendker (1987).

measured by Altenhoff et al. (1994) are clearly in excess of our model. Since we know that P Cyg can vary by as much as 50 per cent in the radio, the excesses seen at millimetre wavelengths may simply be the result of variability (the two millimetre measurements were made relatively close in time). On the other hand, they could conceivably indicate the presence of cold dust in the wind, possibly associated with the outburst two millenia ago. If the latter were really the case, then this cold dust could make a non-negligible contribution to the radio fluxes. Although the slope obtained from the two millimetre-wave fluxes is rather shallower than that of the underlying free-free continuum, it should be borne in mind that the uncertainty on the 3.3-mm flux is quite large, and the beamwidth of the 3.3-mm measurement was 26 arcsec compared with only 11 arcsec for the 1.2-mm observation (which might indicate an extended source for the millimetre-wave flux, consistent with the origin of the underlying continuum). However, the observations at a wavelength of 7 mm by Contreras et al. (1996) are entirely consistent with our model, and also show variability at the several-mJy level consistent with our results at longer wavelengths. The fluxes at 1.2 and 3.3 mm thus appear to be difficult to reconcile with the VLA observations, and further observations should be made to confirm them or search for possible variability. Furthermore, if P Cyg had undergone a red supergiant phase, it would have then had a luminosity far above the observational Humphreys–Davidson limit for massive stars. The nebular velocity of 110 km s^{-1} is also substantially higher than is observed in any red supergiant winds. Thus the red supergiant hypothesis for P Cyg seems unlikely.

The unexpected variability in the morphology of the inner portion of P Cyg’s wind seen in our MERLIN data has been discussed by Skinner et al. (1997b). They showed that, if clumps in the inner wind have densities of order four times higher than the mean, recombination can occur on a time-scale of 40 d or so. They

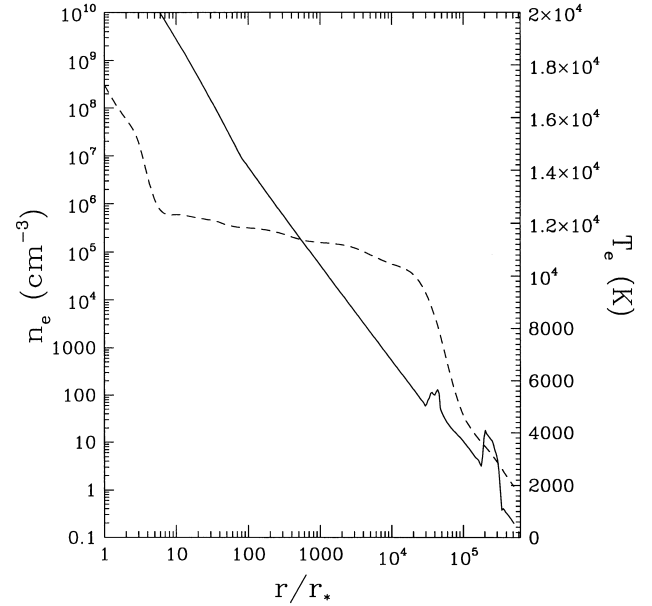


Figure 18. Electron density (solid line) and temperature (dashed line) as functions of radial offset from the centre of the star in units of the stellar radius, for the model used to generate Fig. 17.

also suggested that the simple recombination scheme proposed by van den Oord et al. (1985) probably could not work, but that a variant involving electron temperature variation brought about by the cooling by forbidden and semi-forbidden line emission could indirectly lead to recombination and the observed variability. Our BBI data suggest that some variability can occur on a time-scale of only a few days. For the entire wind to change flux substantially on this time-scale, using the above recombination mechanism, the electron density would have to be about 40 times higher in blobs or shells. However, the BBI data typically show only small variations, so that it is possible that the real time-scale is much longer than a few days, and that what we observe is the chaotic combination of simultaneously increasing and decreasing flux contributions from different regions of the wind with different densities.

In generating our deep VLA images, we have scaled the individual data sets to account for the observed variability of the source at 2 and 6 cm. The only mechanism we have been able to suggest that might explain the rapid variability is that suggested by van den Oord et al. (1985) involving a variable ionization fraction in the wind. This mechanism can significantly affect the radio flux emanating from the compact core where the electron density is high, but in the outer parts of the nebula the electron density is too low, so that the recombination time-scale is far too long for such a mechanism to generate any significant variability. In addition, the outer nebula is several light-months in radius, so that any radiatively driven effect in this region would in any case suffer a considerable time ‘smearing’ owing to the long light travel time. The entire visibility function will be adjusted whether the variability is confined to the core of the nebula or affects the entire source. However, if only the core changes its radio flux the visibility function will be adjusted by some additive amount (either positive or negative), whereas if the entire radio source changes flux the visibility function is adjusted by some multiplicative factor (which can be greater than or less than unity). Although it is clear in the individual observational data sets that the visibility curve is changing from one date to another,

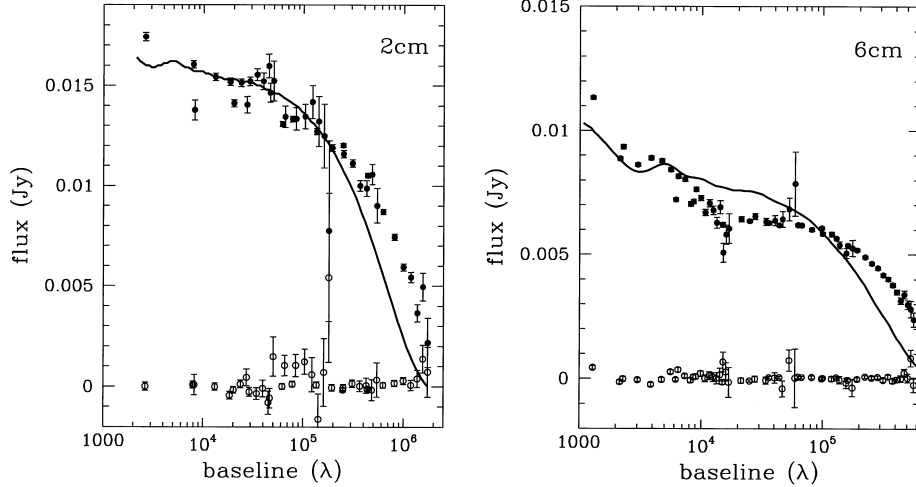


Figure 19. Fit of the model (solid lines) to the observed visibility curves at 2 and 6 cm (error bars).

the S/N is not in general high enough to determine whether the change is additive or multiplicative. If we were to use a multiplicative factor when we should have used an additive one, the effects should be relatively minor since *in general* the flux changes are only at the $\approx \pm 20$ per cent level (although there are some larger excursions), and our images are obtained from the combined visibility set where many of the effects over time should simply cancel out. However, the CLEAN algorithm used to generate the final images in AIPS will produce slightly less accurate results if we have incorrectly scaled the individual data sets. Comparison of our final images with those produced using a combined data set without any scaling at all indicated that the differences were relatively minor, with the structure in the extended nebulosity slightly sharper and therefore of relatively higher surface brightness. The difference between a multiplicative and additive scaling is likely to be smaller still, so that this uncertainty in our results will not be significant. The agreement in detail between our radio images and the optical images of Barlow et al. (1994) confirms this. There is a slight suggestion in our VLA images that the P Cyg radio nebula may be elliptical rather than circular, with its major axis at a position angle of about 120° . This could imply that the P Cyg nebula is axially rather than spherically symmetric, in keeping with the suggestion by Nota, Livio & Clampin (1995). This certainly needs further observation for confirmation, however.

The fit of our model to most of the available observational data is quite good. We fit the radial profile quite well, although we obtain a little too much limb brightening in the 2000-yr-old shell. Our fit to the VLA visibility curves is reasonable. The main problem with both curves is that our model generates too little flux at very long baselines at both wavelengths. This deficiency could probably also be remedied by invoking inhomogeneities in the wind, which will contribute flux at baselines corresponding to the size-scales of the blobs or the resolution of the data, whichever is smaller. Our data imply that the size-scale of the blobs is 40 mas or less, and thus the real wind will provide significant flux at baselines as long as a few M λ . In our simple model, the smallest structure is the radio photosphere, which has a size of order 300 mas at 6 cm, corresponding to about 0.7 M λ . Within the uncertainties introduced by the clear inhomogeneity of the P Cyg envelope and its substantial variability, our model appears to provide a reasonable fit to the observations, and to be physically plausible.

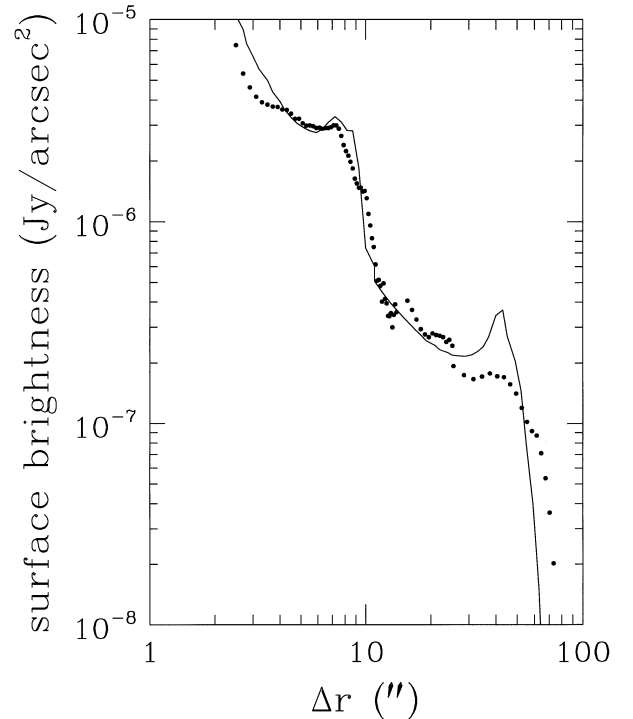


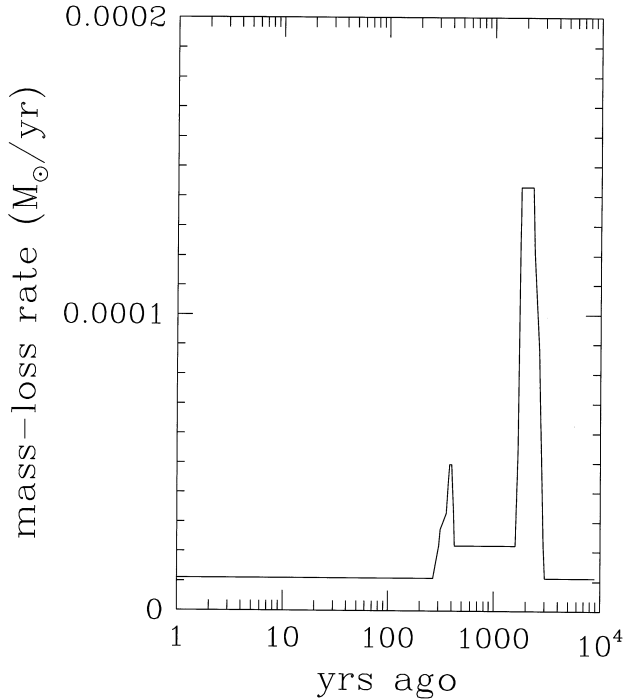
Figure 20. Fit of the model (solid line) to the observed radial profile at 6 cm (filled circles).

8 CONCLUSIONS

Our detailed radio study of P Cyg has shown that it is surrounded by a nebula emitting at 2 and 6 cm which extends to around an arcminute from the star, and that the radio emission varies by ± 20 per cent (and occasionally by significantly more) on time-scales of only a few days. This rather rapid variability might possibly be explained in terms of changes of the ionization structure in the inner part of the circumstellar envelope, but only if the wind contains blobs with very much greater density than the surrounding envelope material. The radio nebula is highly inhomogeneous, appearing to consist of a collection of blobs or filaments, and appears to be dominated by three regions – a compact core only a

Table 4. Model parameters.

Stellar radius	5.6×10^{12} cm
Stellar effective temperature	19000 K
Distance	1800 pc
Mass-loss rate	$1.1 \times 10^{-5} M_{\odot} \text{ yr}^{-1}$
Wind terminal velocity	200 km s^{-1}
Wind velocity near photosphere	20 km s^{-1}
Distance to reach 180 km s^{-1}	4.5×10^{14} cm

**Figure 21.** Mass-loss rate (in solar masses per year) as a function of look-back time (years ago) used for the model. Note the mass-loss outbursts which occurred roughly 400 and 2000 yr ago.

few tenths of an arcsecond in diameter, an inner nebula with a diameter of roughly 18 arcsec which probably corresponds to one or two outburst(s) of increased mass loss during the 17th Century, and an outer nebula with a diameter of roughly 90 arcsec which probably corresponds to an earlier episode of greatly increased mass loss roughly two millenia ago. All the nebular radio emission is consistent with free-free emission by an ionized stellar wind, with the exception of two aberrant observations at 1.2 and 3.3 mm, which should be re-done for confirmation. Our model of the circumstellar envelope suggests that during the most recent outburst, in the 17th Century, the mass-loss rate was probably of order $5 \times 10^{-5} M_{\odot} \text{ yr}^{-1}$, and during the previous outburst the mass-loss rate may have been more than $10^{-4} M_{\odot} \text{ yr}^{-1}$, while the current mass-loss rate is only $1.1 \times 10^{-5} M_{\odot} \text{ yr}^{-1}$. Both of the outbursts represent mass-loss rates entirely consistent with other LBVs or related massive stars.

ACKNOWLEDGMENTS

The National Radio Astronomy Observatory is operated by

Associated Universities, Inc., under contract with the National Science Foundation.

REFERENCES

- Abbott D. C., Bieging J. H., Churchwell E., Cassinelli J. P., 1980, *ApJ*, 238, 196
- Abbott D. C., Bieging J. H., Churchwell E., 1981, *ApJ*, 250, 645
- Abbott D. C., Telesco C. M., Wolff S. C., 1984, *ApJ*, 279, 225
- Altenhoff W. J., Thum C., Wendker H. J., 1994, *A&A*, 281, 161
- Baars J. W. M., Wendker H. J., 1987, *A&A*, 181, 210
- Barlow M. J., Cohen M., 1977, *ApJ*, 213, 737
- Barlow M. J., Drew J. E., Meaburn J., Massey R. E., 1994, *MNRAS*, 268, L29
- Bevington P. R., Robinson D. K., 1992, *Data Reduction and Error Analysis for the Physical Sciences*. McGraw-Hill, New York
- Clampin M., Nota A., Golimowski D. A., Leitherer C., Durrance S. T., 1993, *ApJ*, 410, L35
- Conti P. S., 1984, in Maeder A., Renzini A., eds, *Observational Tests of the Stellar Evolution Theory*. Reidel, Dordrecht, p. 233
- Contreras M. E., Rodríguez L. F., Gómez Y., Velázquez A., 1996, in Taylor A. R., Pareoles J. M., eds, *ASP Conf. Ser. Vol. 93, Radio Emission from the Stars and the Sun*. Astron. Soc. Pac., San Francisco p. 29
- Davidson K., Dufour R. J., Walborn N. R., Gull T. R., 1986, *ApJ*, 305, 867
- Deacon J. R., 1991, PhD thesis, Univ. London
- Deacon J. R., Barlow M. J., 1991, in van der Hucht K. A., Hidayat B., eds, *Wolf-Rayet Stars and Interrelations with Other Massive Stars in Galaxies*. Reidel, Dordrecht, p. 558
- de Groot M. J. H., 1969 *Bull. Astron. Inst. Neth.*, 20, 225
- Drew J. E., 1985, *MNRAS*, 217, 867
- Goodman R., 1957, *Teach Yourself Statistics*. English Universities Press Ltd
- El Eid M. F., Hartmann D. H., 1993, *ApJ*, 404, 271
- Humphreys R. M., 1989, in Davidson K., Moffat A. F. J., Lamers, H. J. G. L. M., eds, *Physics of Luminous Blue Variables*. Kluwer, Dordrecht, p. 3
- Johnson D. R. H., Barlow M. J., Drew J. E., Brinks E., 1992, *MNRAS*, 255, 261
- Klein R. I., Castor J. I., 1978, *ApJ*, 220, 902
- Lamers H. J. G. L. M., de Groot M. J. H., 1992, *A&A*, 257, 153
- Lamers H. J. G. L. M., de Groot M. J. H., Cassatella A., 1983, *A&A*, 123, L8
- Lamers H. J. G. L. M., Korevaar P., Cassatella A., 1985, *A&A*, 149, 29
- Leitherer C., Zickgraf F. J., 1987, *A&A*, 174, 103
- Nota A., Leitherer C., Clampin M., Greenfield P., Golimowski D. A., 1992, *ApJ*, 398, 621
- Nota A., Livio M., Clampin M., 1995, *ApJ*, 448, 788
- Padin S., Davis R. J., Lasenby A. N., 1987, *MNRAS*, 224, 685
- Panagia N., Felli M., 1975, *A&A*, 39, 1
- Pauldrach A. W. A., Puls J., 1990, *A&A*, 237, 409
- Skinner C. J., Whitmore B., 1988, *MNRAS*, 235, 603
- Skinner C. J., Dougherty S. M., Meixner M., Bode M. F., Davis R. J., Drake S. A., Arens J. F., Jernigan J. G., 1997a, *MNRAS*, 288, 295
- Skinner C. J., Exter K. M., Barlow M. J., Davis R. J., Bode M. F., 1997b, *MNRAS*, 288, L7
- Underhill A. B., 1979, *ApJ*, 234, 528
- van den Oord G. H. J., Waters L. B. F. M., Lamers H. J. G. L. M., Abbott D. C., Bieging J. H., Churchwell E., 1985, in Hjellming R. M., Gibson, D. M., eds, *Radio Stars*. Reidel, Dordrecht p. 111
- Waters L. B. F. M., Wesseliuss P. R., 1986, *A&A*, 155, 104
- Wendker H. J., 1982, *A&A*, 116, L1
- Wendker H. J., Baars J. W. H., Altenhoff W. J., 1973, *Nature Phys. Sci.*, 245, 118
- White R. L., Becker R. H., 1982, *ApJ*, 262, 657
- Wright A. E., Barlow M. J., 1975, *MNRAS*, 170, 41

This paper has been typeset from a $\text{T}_{\text{E}}\text{X}/\text{L}^{\text{A}}\text{T}_{\text{E}}\text{X}$ file prepared by the author.